

Fetal gene therapy for neurodegenerative disease of infants

Authors: Giulia Massaro¹, Citra N.Z. Mattar², Andrew M.S. Wong³, Ernestas Sirka⁴, Suzanne M.K. Buckley⁵, Bronwen R. Herbert⁶, Stefan Karlsson⁷, Dany P. Perocheau⁵, Derek Burke¹⁴, Simon Heales¹⁴, Angela Richard-Londt⁸, Sebastian Brandner⁸, Mylene Huebecker⁹, David A. Priestman⁹, Frances M. Platt⁹, Kevin Mills⁴, Arijit Biswas², Jonathan D. Cooper^{3,15,16}, Jerry K.Y. Chan^{2,10,11}, Seng H. Cheng¹², Simon N. Waddington^{5,13,*}, Ahad A. Rahim¹

Affiliations:

¹UCL School of Pharmacy, University College London, London, UK.

²Department of Obstetrics and Gynaecology, Yong Loo Lin School of Medicine, National University of Singapore, Singapore.

³Department of Pediatrics, Washington University School of Medicine, 660 South Euclid Avenue, Campus Box 8208, St. Louis, MO 63110.

⁴UCL Great Ormond Street Institute of Child Health, University College London, London, UK.

⁵UCL Institute for Women's Health, University College London, UK.

⁶ Institute for Reproductive and Developmental Biology, Imperial College London, London, UK.

⁷Division of Molecular Medicine and Gene Therapy, Lund University, Lund, Sweden.

⁸Department of Neurodegenerative Disease, UCL Institute of Neurology, University College London, London, UK.

⁹Department of Pharmacology, University of Oxford, Oxford, UK.

¹⁰Department of Reproductive Medicine, KK Women's and Children's Hospital, Singapore

¹¹Cancer and Stem Cell Biology, Duke-NUS Medical School, Singapore

¹²Sanofi, Framingham, MA 01701, USA.

¹³MRC Antiviral Gene Therapy Research Unit, Faculty of Health Sciences, University of the Witwatersrand, Johannesburg, South Africa.

¹⁴Paediatric Laboratory Medicine, Great Ormond Street Hospital and UCL Great Ormond Street Institute of Child Health, London

¹⁵Department of Basic and Clinical Neuroscience, King's College London, Institute of Psychiatry, Psychology & Neuroscience, London, UK

¹⁶Department of Pediatrics, Washington University School of Medicine, St. Louis, MO 63110

*Correspondence to: s.waddington@ucl.ac.uk

Introduction

For inherited genetic diseases, fetal gene therapy offers the potential of prophylaxis against early, irreversible and lethal pathological change. To explore this, we studied neuronopathic Gaucher disease (nGD), caused by mutations in *GBA*. In adult patients, the milder form presents with hepatomegaly, splenomegaly and occasional lung and bone disease; this is managed, symptomatically, by enzyme replacement therapy. The acute childhood lethal form, nGD is untreatable since enzyme cannot cross the blood brain barrier. nGD patients exhibit signs consistent with hindbrain neurodegeneration including neck hyperextension, strabismus and, often, fatal apnea¹. We selected a mouse model of nGD carrying a loxP-flanked neomycin disruption of *Gba* plus Cre recombinase regulated by the keratinocyte-specific K14 promoter. Exclusive skin expression of *Gba* prevents fatal neonatal dehydration. Instead, mice develop fatal neurodegeneration within fifteen days². Using this model, fetal intracranial injection of adeno-associated virus (AAV) vector reconstituted neuronal GCCase expression. Mice lived for up to at least 18 weeks, were fertile and fully mobile. Neurodegeneration was abolished and neuroinflammation ameliorated. Neonatal intervention also rescued mice but less effectively. As the next step to clinical translation, we also demonstrated the feasibility of ultrasound-guided global AAV gene transfer to fetal macaque brains.

Main text

Antibodies against activated microglia (CD68) and astrocytes (glial fibrillary acid protein, GFAP) were used to assess spatiotemporal neuroinflammation and gliosis in the nGD mouse and this was quantified by thresholding image analysis. Unlike wild types (WT) and heterozygotes, brains of symptomatic P12 knockouts exhibited significant and widespread microglial activation (Fig. S1C) particularly in the gigantocellular nucleus (Gi) of the brainstem, the ventral posteromedial and posterolateral thalamic nuclei (VPM/VPL) and layer V of the somatosensory barrel field cortex (Layer V S1BF). Blinded semi-quantitative scoring revealed that no region was spared (table S1). This was confirmed by immunostaining for a second microglial marker, Iba1 (Fig. S1F). Significant astrogliosis (Fig. S2C), was confirmed by both thresholding analysis and blinded scoring (table S2). At presymptomatic age P8, knockout mouse brains showed significant microglial (Fig. S1B) and astrocyte (Fig. S2B) activation in the thalamus and brainstem. Blinded scoring (tables S1 and S2) and Iba1 immunohistochemistry (Fig. S1E) provided confirmation. Remarkably, even in P1 neonates there was significant activation of astrocytes (Fig. 1A, 1B and 1C) and microglia (Fig. 1D, 1E and 1F) in the brainstem.

Neuronal loss was quantified by stereological assessment of Nissl stained coronal sections. There was significant neuronal loss in the cortex, thalamus and brainstem of knockouts at P12 (Fig. S3B), accompanied by acellular spaces consistent with either large vacuole formation or lipid accumulation as determined by hematoxylin and eosin staining (Fig. S3C). In P8 knockouts there was significant loss of cortical and midbrain neurons (Fig. S3A). Neuronal loss correlated with microglial and astrocyte activation and, consistent with findings in a milder nGD model³ there was significant cortical thinning in S1BF (Fig. S3D), however no difference in volume was observed (Fig. S3E).

In the absence of functional GCCase, its substrate, glucosylceramide (D-glucosyl- β 1-1'-Nacyl-D-erythro-sphingosine), and related sphingolipid species accumulate in both humans and mouse models⁴. Total glucosylceramide and glucosylsphingosine are elevated >20 fold at birth in the nGD mouse⁵, but no detailed measurements of different glucosylceramide species and proximal metabolites have been made. We assembled a temporal profile in whole

brain homogenates using liquid chromatography and tandem mass spectrometry. In knockouts all glucosylceramide species except for C24:0-OH and C24:1-OH were significantly elevated at P1, C18:0 and C16:0 being most abundant (Fig 1G and Fig. S4A); glucosylpsychosine was increased the most (table S3). At P8 and P12 these remained the most elevated in both absolute (Fig. S4B and S4C) and relative (table S3) terms. As expected, the gangliosides GM1a, GD1a, GD1b or GTb remained unchanged in knockouts irrespective of their age (fig S4D to S4F).

The upregulation of neuroinflammatory markers and glycosphingolipids in P1 knockouts suggested that prophylactic *in utero* gene therapy might be beneficial. We selected adeno-associated virus serotype 9 (AAV9) as we⁶, and others⁷ have observed widespread neuronal expression of green fluorescent protein (GFP), following fetal intracranial injection. We examined the expression profile after fetal intracranial injection of an AAV9 vector encoding GFP driven by a β -glucuronidase (GUSB) promoter⁸ (Fig. S5A). At 16 days gestation fetuses received 5 μ l of AAV9 vector (5×10^{10} genome copies) into the lateral ventricle. At 30 days of age, strong bilateral fluorescence extended from the olfactory bulbs to the brainstem (Fig. S5B). Bilateral homogeneity of expression and extensive spread from prefrontal cortex to cerebellum and brainstem was confirmed by immunohistochemistry (Fig. S5C). Many GFP-expressing cells with neuronal morphology were observed in the cortex, striatum, hippocampus, thalamus, cerebellum and, importantly, brainstem (Fig. S5D).

Using the same vector configuration, mode and timing of injection we delivered human AAV9-GBA⁹ into pups of *Gba* heterozygous parents. Whilst impossible to genotype *in utero*, we identified three knockouts after birth by assay of GCase activity in blood spots obtained by superficial temporal vein puncture. They exhibited neither paralysis nor dyskinesia, remaining indistinguishable from WT littermates until sacrifice at 35 days of age. Treated knockouts had substantially diminished microglial and astrocyte activation versus untreated P12 knockouts in the prefrontal cortex, striatum, hippocampus and cerebellum (Fig. 2A and 2B and Fig. S6A and S6B) and there was a tendency for greater treatment effects in Gi than S1BF (Fig. S6D and S6E).

Lysosomal-associated membrane protein 1 (LAMP-1) is increased in fibroblasts of a patient with nGD¹⁰, and was, therefore, selected as a more direct marker of lysosomal compartment size. P12 knockout brains showed strong LAMP-1 expression compared with P35 WT mice. In contrast, staining was similar in treated knockouts and WT mice, with the exception of few, sparse darkly stained LAMP-1 positive cells in treated knockouts (Fig. 2C and Fig. S6C)

Gene therapy prevented neuronal loss in knockouts in the thalamus and Gi (Fig. 2D). Staining with two anti-GCase antibodies indicated that normal enzyme expression had been restored, yet each provided different insights. A C-terminus-specific antibody showed that WT and AAV9-treated knockouts exhibited discrete GCcase immunoreactivity within neurons, that was completely absent in untreated knockouts. In contrast, an N-terminal antibody revealed strong staining of glia rather than neurons in all cortical layers, which was absent in WT brains. After AAV9 treatment of knockouts, staining was observed in neurons in the deeper cortical layers but not in glia (Fig. 2E).

To test long-term efficacy, we injected five knockouts (two males and three females, three separate litters). Consistent with the description of the model², seven untreated control knockouts developed forelimb paralysis then tetraparesis; 5 and 2 mice were sacrificed at humane endpoints at 14 and 15 days of age. In contrast, at 70 days of age all treated

knockouts appeared normal and fertile, two were able to produce a litter of two symptomatic knockouts (movie S1). One treated mouse was culled at 125 days after exhibiting stereotypic circling behavior and another at 131 days because of an untreatable eye infection; at which time the remainder were then culled (Fig. 2F). GCase activity in brain homogenates of treated mice was not significantly different from WTs (Fig. 2G). Paradoxically, other parameters indicated only partial correction of disease phenotype. Treated knockouts tended to perform worse on rotarod (Fig. 2H) and grid walk (Fig 2I) tests. At 100 days they weighed significantly less than unaffected littermates (Fig. 2J) and appeared hyperkinetic (movie S2). They exhibited significant elevation of the shorter chain glycosphingolipids, glucosylpsychosine and lyso-lactosyl ceramide (Fig. 2K) and GD1a (Fig. S6G) but not glucosylceramide (fig S6H). Microglial activation (Fig. S6I) and astrogliosis (Fig. S6J) was ameliorated but not normalized and four of the five mice exhibited ventriculomegaly.

To test efficacy of gene therapy later in development, newborn (P0-P1) knockouts received intracerebroventricular injection of 5 μ l AAV9 vector (5.0×10^{10} genome copies). Previous studies have demonstrated the ability of intravenous AAV9 to cross the blood-brain barrier of neonatal mice^{11,12} and non-human primates¹¹ resulting in efficient expression in neural cells and viscera¹³. Therefore, we also tested if an intravenous administration of the AAV9 vector (4×10^{11} genome copies) to knockouts could ameliorate both visceral and brain pathology. Both treated cohorts were rescued from neonatal death, exhibited neither paralysis nor dyskinesia and remained indistinguishable from WTs until sacrifice at 55 days of age (Fig 3A). There were no significant differences in weight (Fig 3B) or motor co-ordination (Fig 3C) between treated knockouts and WTs.

There was significant supraphysiological expression of GCase in the cortical S1BF region, CENT2 of the cerebellum and Gi, and physiological levels in the hippocampal CA1-CA2 and thalamic VPM/VPL regions (Fig. 3D). There was no significant increase in astrogliosis the CA1-CA2, VPM/VPL and Gi of intravenously injected knockouts at 55 days (Fig. 3E) however there was a significant increase in the S1BF, VPM/VPL and CENT2 regions. There was no significant increase in microglial activation between the treated mice in any region except S1BF (Fig. 3F). Furthermore, the untreated 14 day old knockout nGD mice showed a significantly higher amount of staining compared to the older intravenously treated mice in the VPM/VPL and Gi regions. There was no significant increase in the lysosomal marker LAMP1 in any region except Gi (Fig. 3G). There was no significant loss of neurons in the Gi of knockouts mice treated with intravenous gene therapy (Fig. 3H). However, there was a significant loss in the cortical S1BF and thalamic VPM/VPL regions. The cortex was significantly thinner in intravenously-injected knockouts (Fig. 3H). Despite overall strong GCase staining in the S1BF region and the cerebral cortex neuroinflammation, neuronal loss and subsequent cortical thinning were still evident.

After both intracerebroventricular and intravenous injection GCase was significantly elevated in visceral organs (Fig. 3I), suggesting vector escape from the brain after intracerebroventricular administration. Intravenous gene therapy normalized enzyme activity in all visceral organs except the heart where activity was supraphysiological. Intravenous gene therapy prevented splenomegaly (Fig. 3J) and Gaucher cell infiltration in spleen, liver and lungs. In contrast, intracerebroventricular injection failed to prevent Gaucher cell infiltration in spleen (Fig. 3K), liver (Fig. 3L) and lungs (Fig. 3M), as confirmed by immunohistochemistry. Therefore, while intracerebroventricular gene therapy is effective in treating the lethal neuropathology, it does not ameliorate the visceral manifestations.

However, intravenous administration effectively limits both neurological and visceral pathology.

Separate groups were assessed for long-term efficacy. All treated mice survived to at least 180 days and were indistinguishable from age-matched WT mice (Fig. 3N). Spleens from intracerebroventricular injection cohorts were significantly heavier than those receiving intravenous injection (Fig. 3P). Large Gaucher cells were present in the spleens following intracerebroventricular, but not intravenous injection (Fig. 3O).

We next asked whether *in utero* gene delivery could achieve widespread expression in the larger, gyrencephalic primate brain by performing ultrasound-guided delivery of AAV9 vectors to mid-gestation fetal macaques. Cerebrospinal fluid flows from the lateral ventricles through the ventricular system to the central canal of the spinal cord and the subarachnoid cisterns. Therefore, to achieve maximum vector spread, we identified the lateral cerebral ventricles of two-day 58 (0.4G) macaque fetuses by transabdominal ultrasound. Vector was injected into the right lateral ventricle under ultrasound guidance. scAAV9-GUSB-GFP was administered at a concentration of 6.6×10^{12} vg/mL over 60 seconds. Correct delivery was confirmed by observation of transient (10 min) ventricular swelling (Fig 4A). Both macaques presented normally at birth. There was extensive and bilateral rostro-caudal expression of GFP (Fig 4B) with numerous GFP-positive cells of neuronal morphology in the superior frontal and middle temporal gyri, thalamus, hippocampus, uvula and Gi (Fig 4C). Most other brain regions contained immunopositive cells except for, particularly, the caudate nucleus and putamen (Fig. S7). No discrete cells were observed in unstained brain (Fig 4B and 4C and Fig. S7).

The sustained, widespread gene expression from a single vector injection is supported by a recent study in non-human primate studies and clinical trials. At least 15 years of AAV-mediated transgene expression has been demonstrated in a non-human primate model of Parkinson's Disease¹⁴. Proof-of-concept has already been provided for single dose sustained long-term AAV expression in liver directed gene therapy for the treatment of hemophiliac patients¹⁵.

Widespread CNS gene delivery by fetal intracranial injection offers the best therapeutic potential for inherited early onset neurodegenerative diseases affecting the whole brain. Delivery to the developing CNS may be especially important since neurons have limited regenerative capacity. This is evidenced by the fact that neonatal vector delivery was less effective than fetal intervention in averting neuronal loss. Of several studies on *in utero* gene therapy in gene-disrupted mice¹⁶, none involved models where pathology is already evident at birth and fetal intervention is the only tractable approach. Recent gene therapy clinical trials for mucopolysaccharidosis type IIIa and spinal muscular atrophy¹⁷ indicate that the youngest patients derived most therapeutic benefit¹⁸.

Normalization of GCase activity in the brain did not completely abolish pathology. Knockouts receiving intracerebroventricular injection developed visceral disease. Hypermetabolism, previously identified in Gaucher patients¹⁹, may account for their lower body mass. However, this would not explain the failure to normalize brain glycosphingolipids, nor prevent long-term microglial and astrocyte activation and ventriculomegaly. AAV gene delivery follows a Poisson distribution²⁰. Therefore, individual neurons may receive variable gene dosage, with some remaining un-transduced, as evidenced by heterogeneous staining in treated knockout brains (Fig. 2E).

Human fetal gene therapy necessitates accurate prenatal diagnosis. From cell-free fetal DNA in the maternal circulation, founder mutations underlying Gaucher disease can be detected non-invasively²¹. Concerns over weak genotype-phenotype correlation can be mitigated: several lysosomal storage diseases, including Gaucher disease, have been diagnosed by enzyme assay of chorionic villi samples²². Currently, prenatal screening is usually restricted to a family with a history of Gaucher disease or parents of an affected child, although advances in non-invasive prenatal diagnosis may help identify most cases.

Perinatal gene transfer has been shown to reduce or avoid an immune response to either a protein, (absent in an animal model and potentially also in some patients), or to a viral capsid protein^{23,24}. Immune tolerance may permit vector readministration. The presence of GCase in the skin of the knockout nGD mice precluded us from investigating this specifically. Nevertheless, immune tolerance towards a non-mammalian protein following fetal or neonatal gene delivery has been observed in non-human primate studies²⁵ and in mice this allowed effective re-administration of vector²⁶. Avoidance of an immune response following gene therapy is important. Non-human primates seropositive for AAV9 are less efficiently transduced using an AAV9 vector²⁷. Prednisolone was used in a recent AAV9 gene therapy clinical trial for spinal muscular atrophy to manage anti-vector immune responses¹⁷. While this effectively managed the immune response, *in utero* administration of vector may preempt exposure to WT AAV and thus development of anti-capsid immunity.

This study highlights the potential of fetal gene therapy for neonatal lethal neurodegenerative diseases; the non-human primate data offers a clinically feasible protocol for its implementation. This, and other preclinical fetal gene therapy studies, address the suggested requirements of the NIH recombinant DNA advisory committee²⁸, namely safety and efficacy in relevant models for progression to clinical trials.

Acknowledgements

SNW, AAR and JDC received funding from UK Medical Research Council grant G1000709. SNW received funding from MR/N019075/1 and MR/P026494/1 and SPARKS (17UCL01). AAR and SNW received funding from MRC grants MR/R015325/1 and MR/N026101/1, NC3Rs grant NC/L001780/1. GM, AAR and SNW received funding from the UK Gauchers Association. AAR received funding from the European Union's Horizon 2020 research and innovation programme under grant agreement No. 666918 (BATCure), Action Medical Research (GN2485), MRC grant MR/M00676X/1, Asociación Niemann Pick de Fuenlabrada, Niemann-Pick UK, Niemann Pick Research Foundation and the NBIA Disorders Association. SMKB and SNW received funding from ERC grant "Somabio" 260862. CNZM received salary support from the Singapore Ministry of Health's National Medical Research Council NMRC/TA/0003/2012 and NMRC/CSA-INV/0012/2016. MH is supported by Parkinson's UK grant H-1501. FMP is a Royal Society Wolfson Research Merit Award holder and a Wellcome Trust Investigator in Science. FMP and DAP were supported by the Mizutani Foundation for Glycoscience. JKYC is funded by Singapore's Ministry of Health's National Medical Research Council NMRC CSA/043/2012, CSA(SI)/008/2016 and CIRG/1459/2016. JDC received funding from the European Union's Horizon 2020 research and innovation programme under grant agreement No. 666918 (BATCure), the Batten Disease Support and Research Association (US) and Batten Disease Family Association (UK). KM received funding from the Peto Foundation. SB was supported by the National Institute of Health Research (NIHR) UCLH/UCL Biomedical Research Centre. We thank R Baker, M Choolani, N Johana, N Wen, B Warburton, S Richards, T O'Mahoney, G Sturges O Woolmer, E-H

Davies, T Collin-Histed, A Mehta, D Hughes. Most of all, for guidance, mentorship and inspiration, we thank C Coutelle.

Author Contributions

G.M contributed murine analysis, immunohistochemistry, manuscript drafting. C.N.Z.M contributed NHP work, manuscript drafting. A.M.S.W contributed immunohistochemistry. E.S. contributed mass spectrometry. S.M.K.B contributed murine analysis B.R.H contributed murine analysis S.K. contributed manuscript drafting D.P.P contributed murine analysis D.B. and S.H. contributed blood spots A.R-L contributed immunohistochemistry S.B contributed immunohistochemistry, manuscript drafting. M.H., D.A.P contributed immunohistochemistry F.M.P. contributed immunohistochemistry, manuscript drafting. K.M. contributed mass spectrometry, manuscript drafting. A.B. contributed NHP work J.D.C contributed immunohistochemistry manuscript drafting. J.K.Y.C contributed NHP work, manuscript drafting. S.H.C contributed vector generation S.N.W contributed murine analysis, manuscript drafting. A.A.R contributed murine analysis, immunohistochemistry, manuscript drafting

Conflicts of interest

Seng H. Cheng is an employee at Sanofi, a biopharmaceutical company

Data availability

All data generated or analysed during this study are included in this published article (and its supplementary information files). Raw data are available online at doi 10.5281/zenodo.1246085. These data are also available from the corresponding author on reasonable request.

References

1. Gupta, N., Oppenheim, I.M., Kauvar, E.F., Tayebi, N. & Sidransky, E. Type 2 Gaucher disease: phenotypic variation and genotypic heterogeneity. *Blood Cells Mol Dis* **46**, 75-84 (2011).
2. Enquist, I.B., *et al.* Murine models of acute neuronopathic Gaucher disease. *Proc Natl Acad Sci U S A* **104**, 17483-17488 (2007).
3. Farfel-Becker, T., *et al.* Spatial and temporal correlation between neuron loss and neuroinflammation in a mouse model of neuronopathic Gaucher disease. *Hum Mol Genet* (2011).
4. Farfel-Becker, T., *et al.* Neuronal accumulation of glucosylceramide in a mouse model of neuronopathic Gaucher disease leads to neurodegeneration. *Hum Mol Genet* (2013).
5. Cabrera-Salazar, M.A., *et al.* Systemic delivery of a glucosylceramide synthase inhibitor reduces CNS substrates and increases lifespan in a mouse model of type 2 Gaucher disease. *PLoS ONE* **7**, e43310 (2012).
6. Rahim, A.A., *et al.* In utero administration of Ad5 and AAV pseudotypes to the fetal brain leads to efficient, widespread and long-term gene expression. *Gene Ther* **19**, 936-946 (2012).
7. Haddad, M.R., Donsante, A., Zervas, P. & Kaler, S.G. Fetal Brain-directed AAV Gene Therapy Results in Rapid, Robust, and Persistent Transduction of Mouse Choroid Plexus Epithelia. *Mol Ther Nucleic Acids* **2**, e101 (2013).
8. Passini, M.A. & Wolfe, J.H. Widespread gene delivery and structure-specific patterns of expression in the brain after intraventricular injections of neonatal mice with an adeno-associated virus vector. *J Virol* **75**, 12382-12392 (2001).
9. Sardi, S.P., *et al.* CNS expression of glucocerebrosidase corrects {alpha}-synuclein pathology and memory in a mouse model of Gaucher-related synucleinopathy. *Proc Natl Acad Sci U S A* (2011).
10. Zimmer, K.P., *et al.* Intracellular transport of acid beta-glucosidase and lysosome-associated membrane proteins is affected in Gaucher's disease (G202R mutation). *J Pathol* **188**, 407-414 (1999).
11. Foust, K.D., *et al.* Intravascular AAV9 preferentially targets neonatal neurons and adult astrocytes. *Nat Biotechnol* **27**, 59-65 (2009).

12. Rahim, A.A., *et al.* Intravenous administration of AAV2/9 to the fetal and neonatal mouse leads to differential targeting of CNS cell types and extensive transduction of the nervous system. *FASEB J* **25**, 3505-3518 (2011).
13. Mattar, C.N., *et al.* Systemic delivery of scAAV9 in fetal macaques facilitates neuronal transduction of the central and peripheral nervous systems. *Gene Ther* **20**, 69-83 (2013).
14. Sehara, Y., *et al.* Persistent Expression of Dopamine-Synthesizing Enzymes 15 Years After Gene Transfer in a Primate Model of Parkinson's Disease. *Hum Gene Ther Clin Dev* **28**, 74-79 (2017).
15. Nathwani, A.C., *et al.* Long-term safety and efficacy of factor IX gene therapy in hemophilia B. *N Engl J Med* **371**, 1994-2004 (2014).
16. McCain, L. & Flake, A.W. In utero stem cell transplantation and gene therapy – recent progress and the potential for clinical application. *Best Practice & Research Clinical Obstetrics & Gynaecology* (2015).
17. Mendell, J.R., *et al.* Single-Dose Gene-Replacement Therapy for Spinal Muscular Atrophy. *N Engl J Med* **377**, 1713-1722 (2017).
18. Tardieu, M., *et al.* Intracerebral administration of AAV rh.10 carrying human SGSH and SUMF1 cDNAs in children with MPSIIIA disease: results of a phase I/II trial. *Hum Gene Ther* (2014).
19. Barton, D.J., Ludman, M.D., Benkov, K., Grabowski, G.A. & LeLeiko, N.S. Resting energy expenditure in Gaucher's disease type 1: Effect of Gaucher's cell burden on energy requirements. *Metabolism* **38**, 1238-1243 (1989).
20. Prasad, K.M.R., Xu, Y., Yang, Z., Acton, S.T. & French, B.A. Robust cardiomyocyte-specific gene expression following systemic injection of AAV: in vivo gene delivery follows a Poisson distribution. *Gene Ther* **18**, 43-52 (2011).
21. Zeevi, D.A., *et al.* Proof-of-principle rapid noninvasive prenatal diagnosis of autosomal recessive founder mutations. *J Clin Invest* **125**, 3757-3765 (2015).
22. Verma, J., *et al.* Inherited metabolic disorders: prenatal diagnosis of lysosomal storage disorders. *Prenat Diagn* **35**, 1137-1147 (2015).
23. Pearson, E.G. & Flake, A.W. Stem cell and genetic therapies for the fetus. *Semin Pediatr Surg* **22**, 56-61 (2013).
24. Nivsarkar, M.S., *et al.* Evidence for contribution of CD4+ CD25+ regulatory T cells in maintaining immune tolerance to human factor IX following perinatal adenovirus vector delivery. *J Immunol Res* **2015**, 397879 (2015).
25. Tai, D.S., *et al.* Development of operational immunologic tolerance with neonatal gene transfer in nonhuman primates: preliminary studies. *Gene Ther* (2015).
26. Waddington, S.N., *et al.* In utero gene transfer of human factor IX to fetal mice can induce postnatal tolerance of the exogenous clotting factor. *Blood* **101**, 1359-1366 (2003).
27. Gray, S.J., *et al.* Preclinical differences of intravascular AAV9 delivery to neurons and glia: a comparative study of adult mice and nonhuman primates. *Mol Ther* **19**, 1058-1069 (2011).
28. Prenatal gene transfer: scientific, medical, and ethical issues: a report of the Recombinant DNA Advisory Committee. *Hum Gene Ther* **11**, 1211-1229 (2000).

Figure Legends

Fig. 1. Brain disease at birth in nGD mice. (A) GFAP immunostaining in newborn knockouts, heterozygous and WT brains. Scale bar = 1mm (B) Higher magnification of (A) in the somatosensory barrel field cortex (S1BF), ventral posteromedial/posterolateral nuclei (VPM/VPL) and gigantocellular nucleus (Gi). Scale bar = 0.25mm. (C) Quantification of (B) (2-way ANOVA, Tukey's multiple comparison). (D) CD68 immunohistochemistry in newborn knockout, heterozygous and WT brains. Scale bar = 1mm (E) Higher magnification of (D). (F) Quantification of (E) (2-way ANOVA). (G) Mass spectrometry analysis of glucosylceramide isoforms, glucopsychosine and lyso-lactosylceramide in knockouts, heterozygote and WT brains (2-way ANOVA on log-transformed data; Bonferroni's multiple comparison). Numbers of mice are stated under each group. n.s. = not significant

Fig. 2. Fetal gene therapy of nGD mice. (A) CD68, (B) GFAP and (C) LAMP1 brain immunostaining of untreated post-gestational day 12 (P12) knockouts and P35 WT and treated mice from different litters (scale bar = 1mm). (D) Stereological estimates of neuron number in the brains of treated knockout, heterozygote, WT and untreated day 12 knockouts

(2-way ANOVA, Bonferroni's multiple comparison, all versus WT). (Representative of 3 KO replicates shown in Fig. S6) (E) GCCase C-terminal antibody labelling neurons in WTs, knockouts and treated knockout brains. N-terminal antibody staining in WT and treated knockouts (S1BF images, scale bar = 0.25mm). Representative of 3 mice replicates per experimental cohort. (F) Survival studies of treated knockouts compared to untreated knockouts (Mantel-Cox test, n=5 and 7 mice, respectively). (G) GCCase enzyme activity in treated and WT brains (Students one-tailed t-test). (H) Rotarod and (I) foot-fault tests on treated knockout and WT mice (2-way ANOVA, Bonferroni's multiple comparison). (J) Weights of treated and WT mice over time (Students one-tailed t-test on weight at 100 days, WT n=19, KO n=5). (K) Mass spectrometry profiles in the brains of treated knockout and WT mice (2-way ANOVA on log-transformed data, Bonferroni's multiple comparison). Numbers of mice are stated under each group. n.s. = not significant

Fig. 3. Intracerebroventricular and intravenous gene therapy in neonatal nGD mice. (A) Kaplan-Meier survival plot of untreated knockouts, IC gene therapy treated knockouts, IV gene therapy treated knockouts and WTs (Logrank, Mantel-Cox test). (B) Weights of mice from (A). (C) Rotarod assessment of mice from (A) (repeated measures ANOVA). Immunohistochemistry for GBA1 (D), GFAP (E), CD68 (F) and LAMP1 (G) in brains of 55 day old treated knockout and WTs and P12 untreated knockouts in the S1BF, hippocampal cornu ammonus 1 (CA1), the cerebellar central lobule II (CENT2) and Gi (2-way ANOVA, Tukey's multiple comparisons). (H) Neuron counts in the Gi, S1BF and VPM/VPL in treated knockouts and WTs and cortical thickness measurements (2-way ANOVA, Tukey's multiple comparisons). (I) GCCase activity in organs of treated knockouts, WTs, and untreated P12 knockouts (2-way ANOVA, Tukey's multiple comparisons). (J) Spleen weights from mice receiving gene therapy and WTs (1-way ANOVA, Tukey's multiple comparisons). Haematoxylin and eosin staining and CD68 immunohistochemistry of (K) spleens, (L) livers and (M) lungs from intravenously and intracerebroventricularly gene therapy treated and WT mice (white arrows highlight Gaucher cells, scale bar = 0.1mm). (N) Kaplan-Meier survival plot of long-term gene therapy treated and untreated knockouts (Mantel-Cox test). (O) CD68 immunohistochemistry on spleens from (N) and WTs (scale bar = 0.25mm). (P) Spleen weights from (O) (1-way ANOVA, Tukey's multiple comparisons). Numbers of mice are stated under each group. n.s. = not significant

Fig. 4. *In utero* gene delivery to the macaque brain via ultrasound-guided intracerebroventricular injection of vector. (A) Ultrasound images following intracerebroventricular administration over time. (B) Green fluorescent protein immunohistochemistry on brain sections from administered macaques and control. Scale bar = 5mm. (C) Higher magnification examination of (B) Scale bar = 0.25mm. Representative of 2 administered macaques replicates

Online methods

Animal welfare

Mouse procedures and welfare was approved by the University College London Animal Welfare and Ethical Review Board (AWERB) and in accordance with project and personal licenses granted by the UK Home Office and the Animal (Scientific Procedures) Act of 1986. The mouse model for acute neuronopathic Gaucher disease used in this study has been previously described together with all genotyping procedures and primer sequences². Mice

heterozygous for mutation in the *Gba1* gene and carrying the Cre recombinase gene on a C57BL/6 background were outbred onto wild type CD1 mice (Charles River, Harlow, UK) for five generations. The CD1 strain allows for larger litter size and excellent maternal care of pups. The colony was then maintained using breeding pairs heterozygous for the GBA mutation and carrying the Cre-recombinase gene. Macaque procedures and welfare were approved by and performed in accordance with the Institutional Animal Care and Use Committee (IACUC) at the National University of Singapore and Singapore Health Services Pte., Ltd (IACUC 2009-SHS-512). All *in vivo* studies performed in macaques were conducted at the SingHealth Experimental Medicine Centre that has been accredited by the Association for Assessment and Accreditation of Laboratory Animal Care International (AAALAC). Potential dams were screened for pre-existing anti-AAV9 antibodies and seronegative females were time-mated. Pregnancies were confirmed, dated and monitored by ultrasound before and after vector delivery.

Histological and immunohistochemical analyses

Experimental cohorts of mice were culled by terminal transcardial perfusion using phosphate buffered saline (PBS), with the exception of P1 mice culled by decapitation. Macaque brains and spinal cords were harvested following euthanasia using isoflurane and pentobarbitone, cardiac puncture and perfusion of 1% paraformaldehyde.

For free-floating immunohistochemistry-based analyses, the brains were removed and placed into 4% paraformaldehyde solution and stored for 48 hours at 4 °C before being cryoprotected in 30% sucrose for a minimum of 24 hours at 4 °C. The brains were then serial sectioned along the rostro-caudal axis at 40 µm thick sections using a freezing microtome (Thermo Fisher Scientific). Immunohistochemical staining was used to detect gene expression. Endogenous peroxidase activity was quenched by incubating sections in 1% H₂O₂ in TBS solution for 30 min. Following three washes in TBS, sections were incubated for 30 min in a solution of 15% normal serum in TBS-T (0.3% Triton X-100 in TBS). Subsequently sections were incubated at 4 °C overnight in primary antibody in TBS-T/10% serum. After rinsing in TBS, the sections were incubated for 2 h in secondary IgG diluted in TBS-T/10% serum. Sections were then rinsed in TBS and incubated for 2 h in a 1:1000 solution of Vectastain avidin–biotin solution (ABC; Vector Labs, Peterborough, UK). The sections were rinsed in TBS and incubated in 0.05% solution of DAB containing 0.01% H₂O₂. The staining reaction was stopped by adding ice cold TBS. The sections were mounted onto chrome-gelatine-coated Superfrost-plus slides (VWR, Poole, UK) and left to air-dry overnight. The sections were dehydrated in 70% ethanol, cleared in xylene for 30 min before being coverslipped using DPX mounting medium. This protocol was used with the following combinations of primary antibodies, blocking serum and secondary antibodies: Rat anti-mouse CD68 (1:100; AbD Serotec, MCA1957)¹², rabbit serum and rabbit anti-rat (1:1000; Vector Laboratories Inc.); mouse anti-GFAP (1:500; Millipore, MAB3402), goat serum and goat anti-mouse (1:1000; Vector Laboratories Inc.); rabbit anti-LAMP1 (1:200; Abcam, AB24170), goat serum and goat anti-rabbit (1:1000; Vector Laboratories Inc.); mouse anti-GBA1 (N-terminus) (1:150; Origene, TA803361), goat serum and goat anti-mouse (1:1000; Vector Laboratories Inc.); rabbit anti-GBA1 (C-terminus) (1:1000; Sigma-Aldrich, G4171), goat serum and goat anti-rabbit (1:1000; Vector Laboratories Inc.); rabbit anti-GFP (1:10,000; Abcam, AB290), goat serum and goat anti-rabbit (1:1000; Vector Laboratories Inc.), respectively. Brain sections were Nissl stained using cresyl violet. The sections were incubated in 0.05% cresyl violet in 0.05% acetic acid for 30 mins at 60 °C and then washed in de-ionised water. The sections were differentiated through ascending concentrations of alcohol before being cleared in xylene and coverslipped with DPX.

For histology and immunohistochemical staining on paraffin-embedded tissue sections, mice were culled by transcardial perfusion as described above. Brain fixed in 10% buffered formol-saline was embedded in paraffin wax. Microglial activation was examined using an ionized calcium binding adaptor molecule 1 (Iba1) antibody (Wako Pure Chemical Industries, Ltd, 019-19741). Immunohistochemistry was performed on automated immunohistochemistry staining machines (Ventana Medical Systems Inc., Tucson, Arizona) using proprietary secondary detection reagents (Ventana Medical Systems Inc.) before development with 3'3-diaminobenzidine tetrachloride as the chromogen. Conventional methods were used for Harris haematoxylin and eosin staining. Sections were mounted on chrome-gelatine coated slides and air dried overnight. The sections were stained protected from light with filtered 0.1% Mayer Hematoxylin (Sigma-Aldrich) for 10 min. The slides were rinsed in distilled water for 5 min and consequently dipped 12 times in 0.5% Eosin solution. The sections were quickly washed in distilled water and subsequently dehydrated for 30 s in rising concentrations of ethanol (50%, 70%, 95%, 100%). The slides were finally incubated in Histo-clear for 30 min and coverslipped with DPX mountant medium.

Quantitative analysis of histological and immunohistochemical staining

The quantification of immunohistochemical staining within discrete regions of the brain was conducted by a user blinded to the experimental cohorts. 40 non-overlapping RGB images were taken at x40 magnification through four consecutive sections within each region of interest. During image capture all camera and microscope settings were maintained. Regional areas of immunoreactivity were analysed by optical segmentation using *Image Pro-Plus* (Media Cybernetics). The foreground immunostaining was defined by averaging of the highest and lowest signals and the threshold was set and remained unchanged as each consecutive image was analysed. The data is represented as the mean percentage area of immunoreactivity per field for each discrete region. Stereological counts of neurons by optical fractionation and measurement of cortical thickness and volume was performed using *Stereo Investigator* (MBF Biosciences)²⁹. The grid size and the counting frame used for analysing different brain regions were the following: S1BF 150 x 150 µm, 50 x 50 µm; VPM/VPL 175 x 175 µm, 50 x 50 µm; Gi 100 x 100 µm, 50 x 50 µm. Cells were counted using a 100X objective. Efficient sampling was estimated by a coefficient of error between 0.05 and 0.1³⁰. 4 sections for each brain were analysed and the average values of cell counting were used in the calculations.

The mean thickness of the S1BF cortical region was estimated by using the Cavalieri vertical sections principle³¹. The length of 10 parallel consecutive lines intersecting perpendicularly the cerebral cortex, traced from the somatosensory barrel cortical layer 1 to the corpus callosum, was measured. 3 sections of the midbrain region per each brain were analysed and the average values were reported.

Mass spectrometry

Mouse brains were homogenised in water using an Ultraturax T25 probe homogeniser (IKA, Germany). Protein concentrations were determined using bicinchoninic acid (BCA) assay and 200µg were analyzed for glucosylceramide, glucosylpsychosine and lyso-lactosyl ceramide accumulation. The substrates were extracted in 1ml of chloroform/methanol (2:1 v/v) containing 80µg/ml of d4-C16:0-glucosylceramide internal standard which was synthesized in house³². The samples were shaken for 30 min at room temperature before the addition of 200µl of PBS for phase separation. After a 10 min centrifugation at 16,000 g upper and lower phases were collected and 5 µl of each were injected into the ultra-performance liquid chromatography – tandem mass spectrometry (UPLC-MS/MS) system. Glycosphingolipid reference standards (Matreya, USA) was also analyzed to confirm analyte identity.

The samples were injected onto Waters ACQUITY UPLC system (Manchester, UK) operated in partial loop mode and separated on Waters ACQUITY UPLC BEH C18 column (130Å, 1.7 μm, 2.1 mm X 50 mm) under the following gradient conditions: 0.00-0.20→80%A; 0.20-5.00→0.1%A; 5.00-9.00→0.1%A; 9.01-11.00→80%A, where mobile phase A was ddH₂O [0.1% FA]; phase B was methanol and the flow rate was 0.65 ml/min. Column and sample temperatures were kept at 40°C and 10°C respectively. Weak wash solvent was ddH₂O [0.1% FA] and strong wash solvent was acetonitrile:methanol:isopropanol:ddH₂O (1:1:1:1 v/v). The eluting analytes were detected on a Waters XEVO TQ-S triple quadrupole mass spectrometer (Manchester, UK) which was equipped with the electrospray ion source and operated in multiple reaction monitoring (MRM) and positive ion mode (see table S4 for MRM details) with the tune page parameters set to achieve the maximum sensitivity for glycosphingolipids as described previously³³. The data was processed with MassLynx v4.1.

GSL Analysis

Glycosphingolipids (GSLs) from brain homogenates were extracted with chloroform:methanol (1:2, v/v) overnight at 4°C and further purified using solid-phase C18 columns (Telos, Kinesis, UK). GSLs were dried down under nitrogen and treated with either Cerezyme® (Genzyme, Cambridge, MA) to obtain glucose from GlcCer, or ceramide glycanase (prepared *in house* from the medicinal leech *Hirudo medicinalis/verbenae*) to obtain oligosaccharides from other GSLs. Liberated glucose and free glycans were then fluorescently-labelled with anthranillic acid (2AA). Excess 2AA label was removed using DPA-6S SPE columns (Supelco, PA, USA). Purified 2AA-labelled glucose and 2AA-labelled glycans were separated and quantified by normal phase high-performance liquid chromatography (NP-HPLC)³⁴. The NP-HPLC system consisted of a Waters Alliance 2695 separations module and an in-line Waters 2475 multi λ-fluorescence detector set at Ex λ360nm and Em λ425nm. The solid phase used was a 4.6 x 250mm TSK gel-Amide 80 column (Anachem, Luton, UK). Results were normalized to protein content determined using bicinchoninic acid (BCA) assay.

Self-complementary AAV Vectors

The human *GBAI* cDNA was generated by polymerase chain reaction, verified by DNA sequencing and cloned into the Topo plasmid vector (Invitrogen, Carlsbad, CA). A 1.6 kb fragment (containing the open reading frame of the human *GBAI* cDNA and bovine growth hormone polyadenylation signal sequence) was then generated by digesting the plasmid with the restriction enzymes *NcoI* and *SpeI* and subcloned into a shuttle plasmid containing the scAAV2 inverted terminal repeats (ITR) and the 0.4 kb GUSB promoter³⁵ (Fig. S8). Recombinant AAV9 serotype vectors encoding *GBAI* (scAAV9-GUSB-*GBAI*) were generated by the standard triple plasmid transfection method as described previously³⁶. Briefly, cell lysates of transfected 293 cells were clarified by centrifugation and then purified by subjecting the preparations to two cycles of density gradient ultracentrifugation using cesium chloride. The purified recombinant vectors were re-suspended and stored in 10 mM sodium phosphate buffer, pH 7.3, containing 180 mM sodium chloride, and 0.001% pluronic F68.

AAV Administrations to mice and macaques

For marker gene studies we injected CD1 outbred mice. nGD mice were backcrossed onto the CD1 background, to maximize litter sizes and minimize risk of cannibalization.

We have previously described the administration of gene delivery vectors to the brains of fetal mice³⁷ and intracerebroventricular injections to neonates has been described³⁸. We have previously described intravenous administration to neonatal mice¹². Briefly, pregnant

mice carrying pups at 16 days gestation were anaesthetized using isoflurane inhalation anaesthesia and a midline laparotomy was performed to expose the uterus. 5µl of AAV vector (5×10^{10} genome copies) was administered to all fetuses per dam via a transuterine injection targeting the anterior horn of the lateral ventricle of the left hemisphere of the brain. The laparotomy was sutured and mice were provided topical and systemic analgesia and allowed to recover in a warm chamber. The same dose was administered via intracerebroventricular injection to P0 neonates. The intracerebroventricular injections were directed to the anterior horn of the lateral ventricle. The injection site was identified at 2/5 of the distance from the lambda suture to each eye. P0-1 mice were anaesthetised on ice for 30-60 seconds. A 33-gauge needle (Hamilton) was inserted perpendicularly at the injection site to a depth of 3mm and 5µl of vector was slowly administered. The pup was allowed to recover and placed back into the cage. 40µl of AAV vector (4×10^{11} genome copies) of vector was administered P0 neonates by injection of the superficial temporal vein. At postnatal day 0-1 pups were anaesthetised on ice for 30-60 seconds and intravenous injections were performed via the superficial temporal vein using a 33-gauge needle (Hamilton). Once the needle was slowly removed, gentle pressure was applied to the injection site. When the pup fully recovered it was returned to the dam.

Cynomolgus macaques (*Macaca fascicularis*) were used for non-human primate studies. Macaques underwent time-mating and pregnancy confirmed through ultrasound evidence of fetal pole and fetal heart activity. Dating of pregnancy was performed as previously reported (Mattar et al Mol Therapy 2011), and IUGT was performed at 0.4G. After induction of anaesthesia via sevoflurane, a 25G Quincke needle (Becton-Dickenson) was used to target the lateral ventricle closest to the anterior maternal abdomen under continuous ultrasound imaging. Vector was injected as a slow bolus (200-350µl to deliver a total dose of 1.3×10^{12} vg and 2.3×10^{12} vg in each fetus respectively) with ventricular swelling observed as evidence of correct delivery. The needle was removed immediately and the fetus monitored for a further 15 minutes. A male fetus was delivered naturally and a female fetus was delivered by caesarean section and hand-reared as previously reported. Euthanasia and organ harvest was performed on days 0 and 6 respectively under ketamine and isoflurane, via cardiac puncture and exsanguination as previously described³⁹.

Mouse behavioural studies

Mice underwent foot-fault testing (adapted from Lubics et al⁴⁰) and Rotarod testing (adapted from Carter et al,⁴¹) at P35, P73 and P100. The operator was blinded to the genotype of the animals throughout the testing period. Briefly, foot-fault testing involved placing a mouse on a stainless steel grid (41 x 25cm) with a mesh size of 1 x 1 cm, elevated 30cm above the bench surface. The number of times a limb fell through the grid (a foot-fault) within 30 seconds was recorded. Rotarod testing employed a commercially available rotarod (Harvard Apparatus, Cambridge, UK). Mice were placed on the rotating drum under continuous acceleration (from 4-40rpm over 5 minutes), with the latency to fall from the rod, and the speed at which this occurred, measured. Any passive rotations were also noted.

Stereoscopic fluorescence microscopy

GFP expression in various organs was visualized with a stereoscopic fluorescence microscope (MZ16F; Leica, Wetzlar, Germany). Representative images were captured with a digital microscope camera (DFC420 Leica, Wetzlar, Germany) and image analysis software (LAS 4.2; Leica, Wetzlar, Germany). Because of the differences in the sizes of the organs, intensity of signal, and distribution of cells of interest, the images captured were optimized for exposure length and brightness in each case.

GCase Enzyme Assay

GCase activity was determined using the established synthetic substrate, 4-methylumbelliferone- β -glucopyranoside protocol as previously described⁴². Frozen tissue samples were homogenized with distilled water on ice and the total protein concentration was measured using BCA assay. Samples were incubated with the substrate for 2 hours at 37 °C. The reaction was stopped with 1M glycine buffer, pH 10.4. Fluorescence of the standard 1nM 4-methylumbelliferone and the samples was read (FluoStar Optima Plate Reader. Excitation wavelength: 360nm; emission wavelength: 450nm). The enzymatic activity (nmol/hr/ μ) was calculated.

Sample sizes, statistics and randomization

Since the genotypes of injected mice could not be ascertained until after birth, the initial sample size was determined by the number of knockout pups in the uteri of three randomly-selected pregnant dams. For most analyses, one-way or two-way analysis of variance (ANOVA) was performed with either Bonferroni or Tukey's multiple comparison. The F statistic, underlying ANOVA is tolerant of violations in normality, for which we did not test. Nevertheless, mass spectrometry data, which was clearly not normally distributed, was converted by log transformation before ANOVA. Each experiment was performed only once. Behavioral and semi-quantitative scoring were blinded to the investigator.

Methods Only References

29. Pressey, S.N., Smith, D.A., Wong, A.M., Platt, F.M. & Cooper, J.D. Early glial activation, synaptic changes and axonal pathology in the thalamocortical system of Niemann-Pick type C1 mice. *Neurobiol Dis* **45**, 1086-1100 (2012).
30. Gundersen, H.J., Jensen, E.B., Kieu, K. & Nielsen, J. The efficiency of systematic sampling in stereology--reconsidered. *Journal of microscopy* **193**, 199-211 (1999).
31. Baddeley, A.J., Gundersen, H.J. & Cruz-Orive, L.M. Estimation of surface area from vertical sections. *Journal of microscopy* **142**, 259-276 (1986).
32. Mills, K., Eaton, S., Ledger, V., Young, E. & Winchester, B. The synthesis of internal standards for the quantitative determination of sphingolipids by tandem mass spectrometry. *Rapid communications in mass spectrometry : RCM* **19**, 1739-1748 (2005).
33. Auray-Blais, C., *et al.* Urinary biomarker investigation in children with Fabry disease using tandem mass spectrometry. *Clinica chimica acta; international journal of clinical chemistry* **438**, 195-204 (2015).
34. Neville, D.C., *et al.* Analysis of fluorescently labeled glycosphingolipid-derived oligosaccharides following ceramide glycanase digestion and anthranilic acid labeling. *Analytical biochemistry* **331**, 275-282 (2004).
35. Passini, M.A., *et al.* Antisense oligonucleotides delivered to the mouse CNS ameliorate symptoms of severe spinal muscular atrophy. *Sci Transl Med* **3**, 72ra18 (2011).
36. Ayuso, E., *et al.* High AAV vector purity results in serotype- and tissue-independent enhancement of transduction efficiency. *Gene Ther* **17**, 503-510 (2010).
37. Rahim, A.A., *et al.* Efficient gene delivery to the adult and fetal CNS using pseudotyped non-integrating lentiviral vectors. *Gene Ther* **16**, 509-520 (2009).
38. Kim, J.Y., Grunke, S.D., Levites, Y., Golde, T.E. & Jankowsky, J.L. Intracerebroventricular viral injection of the neonatal mouse brain for persistent and widespread neuronal transduction. *J Vis Exp* (2014).
39. Mattar, C.N., Biswas, A., Choolani, M. & Chan, J.K. Animal models for prenatal gene therapy: the nonhuman primate model. *Methods in molecular biology (Clifton, N.J.)* **891**, 249-271 (2012).
40. Lubics, A., *et al.* Neurological reflexes and early motor behavior in rats subjected to neonatal hypoxic-ischemic injury. *Behav Brain Res* **157**, 157-165 (2005).
41. Carter, R.J., Morton, J. & Dunnett, S.B. Motor coordination and balance in rodents. *Current protocols in neuroscience / editorial board, Jacqueline N. Crawley ... [et al.]* **Chapter 8**, Unit 8.12 (2001).

42. Wenger, D.A., Clark, C., Sattler, M. & Wharton, C. Synthetic substrate beta-glucosidase activity in leukocytes: a reproducible method for the identification of patients and carriers of Gaucher's disease. *Clinical genetics* **13**, 145-153 (1978).

Figure 1

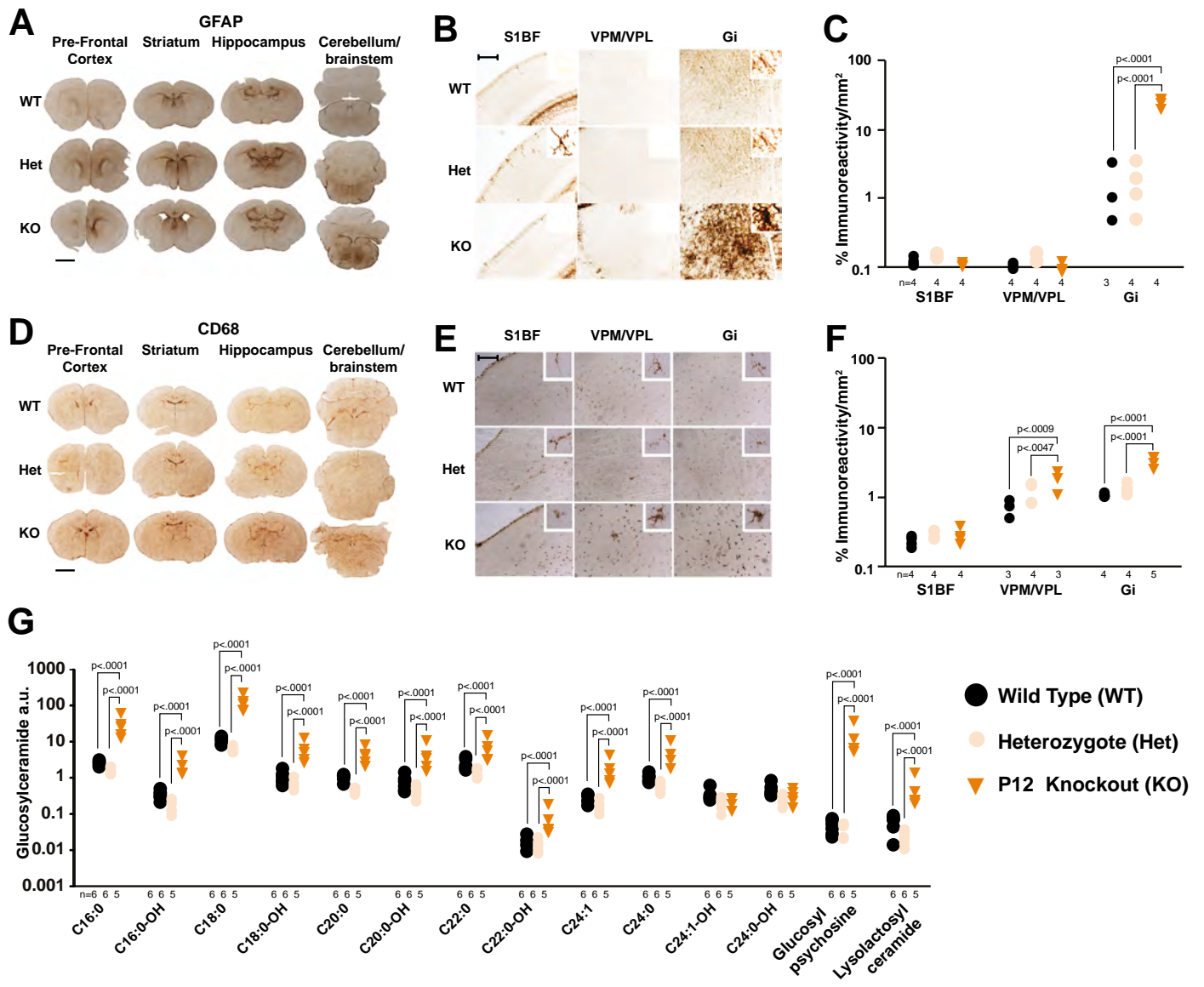


Figure 2

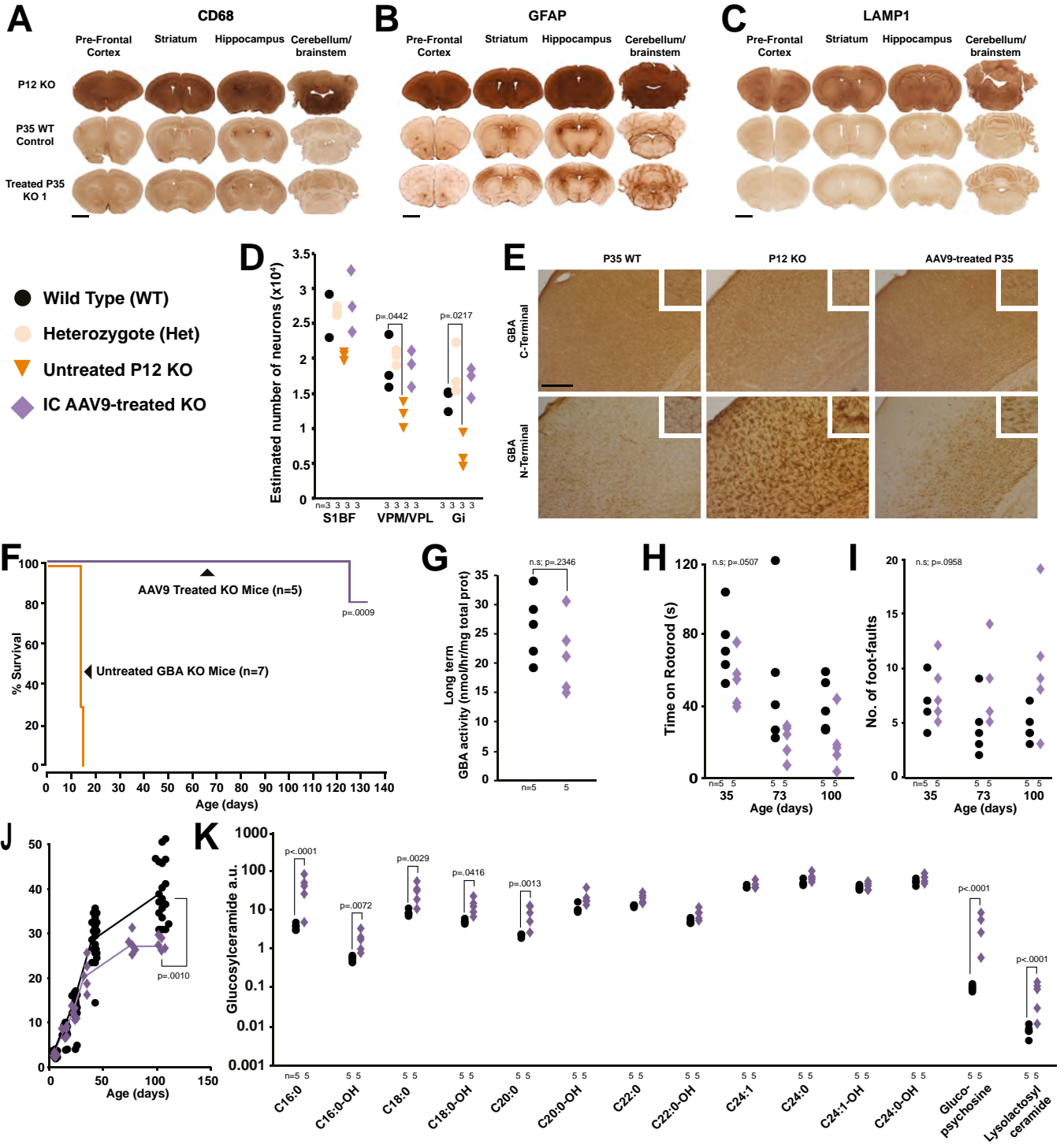


Figure 3

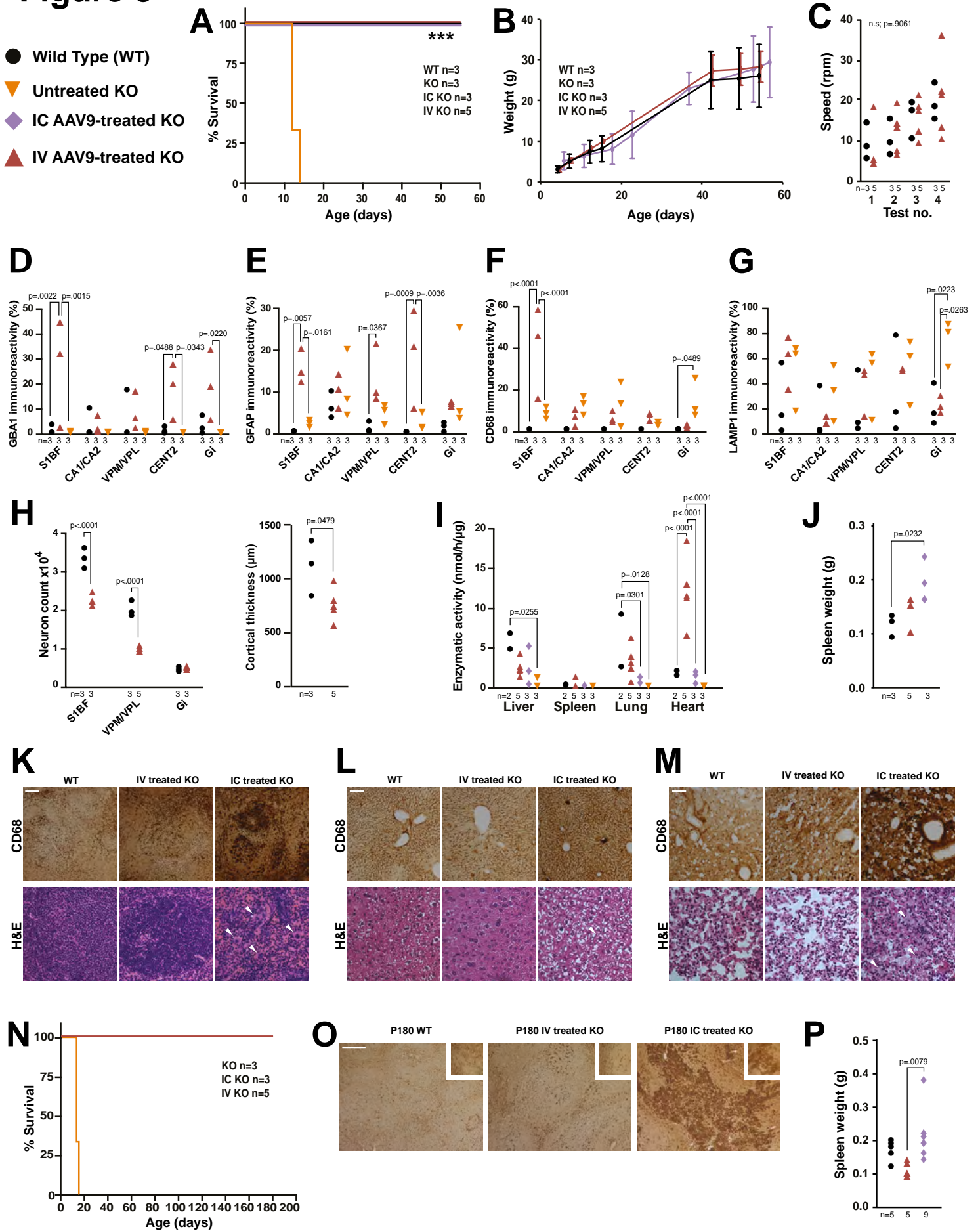
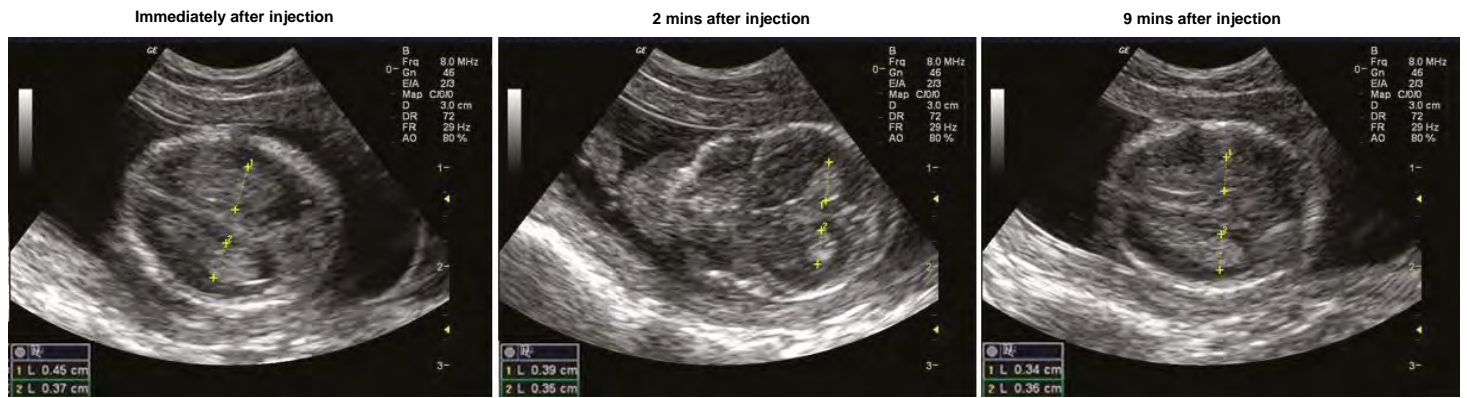
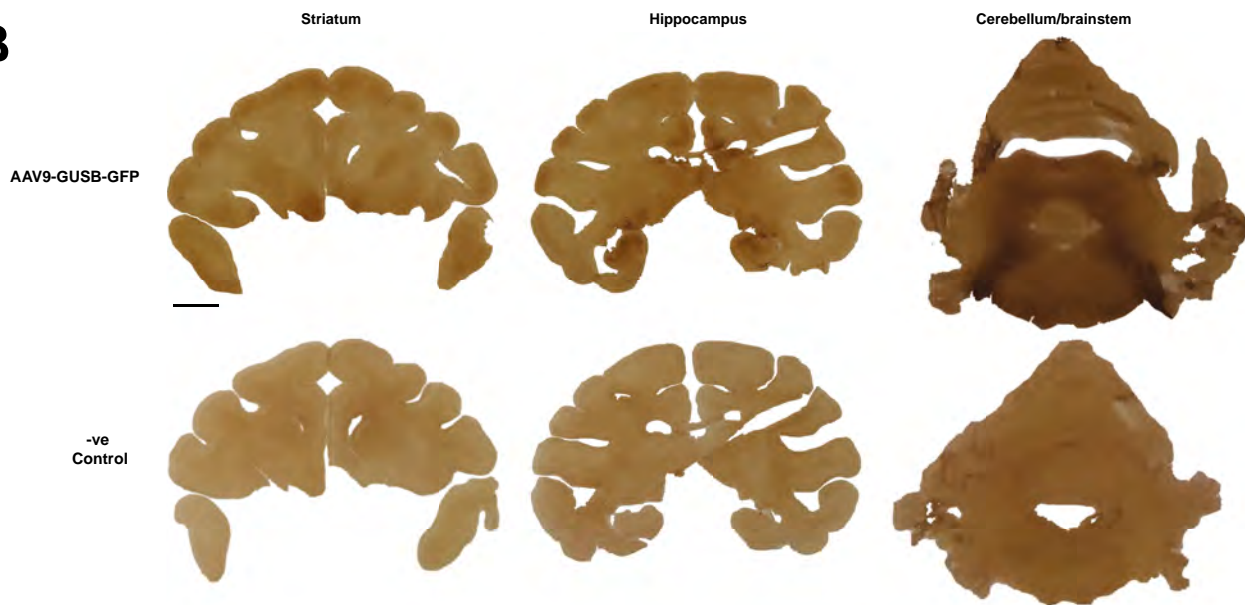


Figure 4

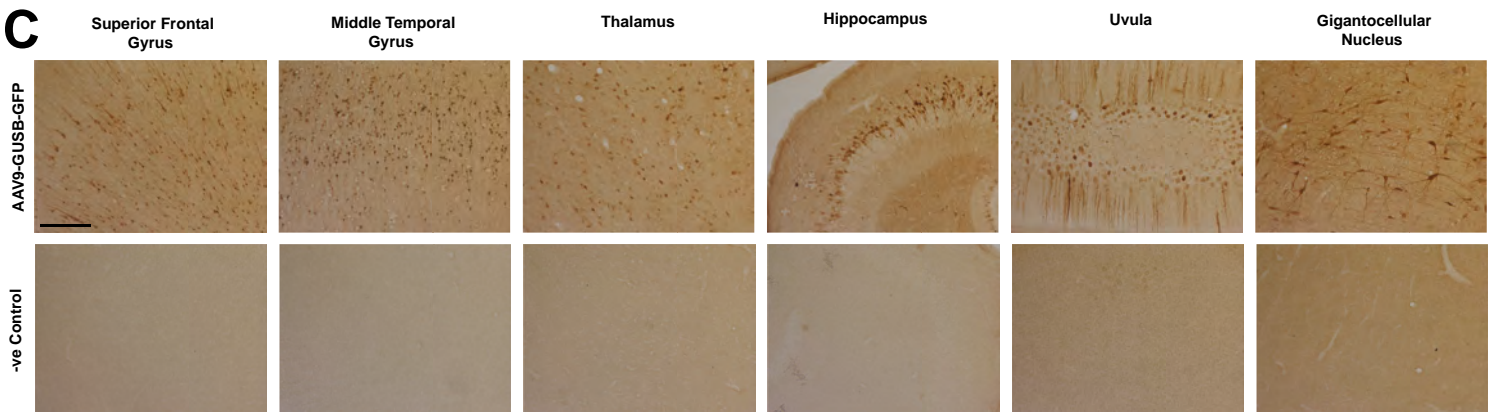
A



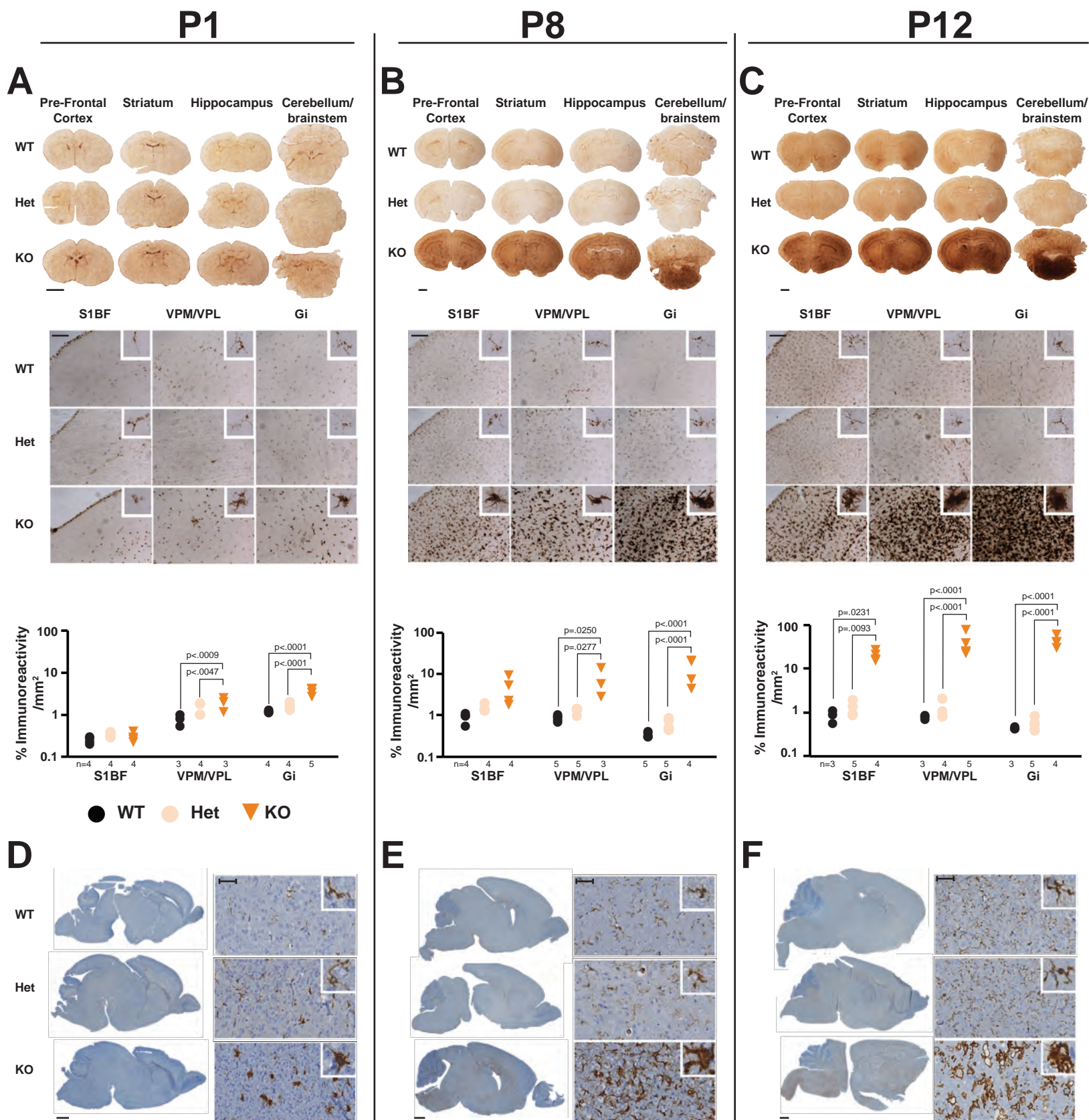
B



C



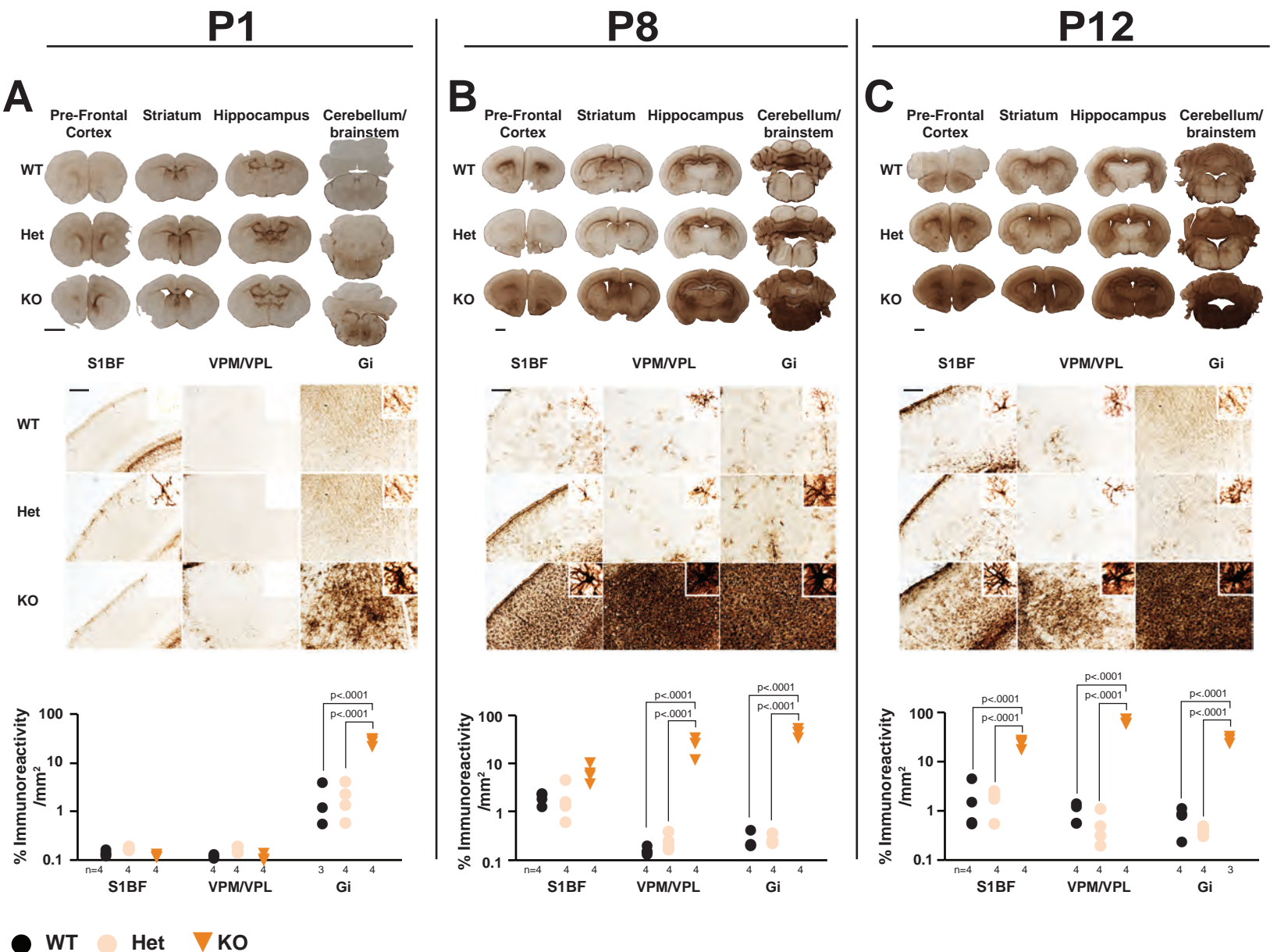
Supplementary Fig. 1



Supplementary Fig. 1. Microglia-mediated inflammation in nGD mice.

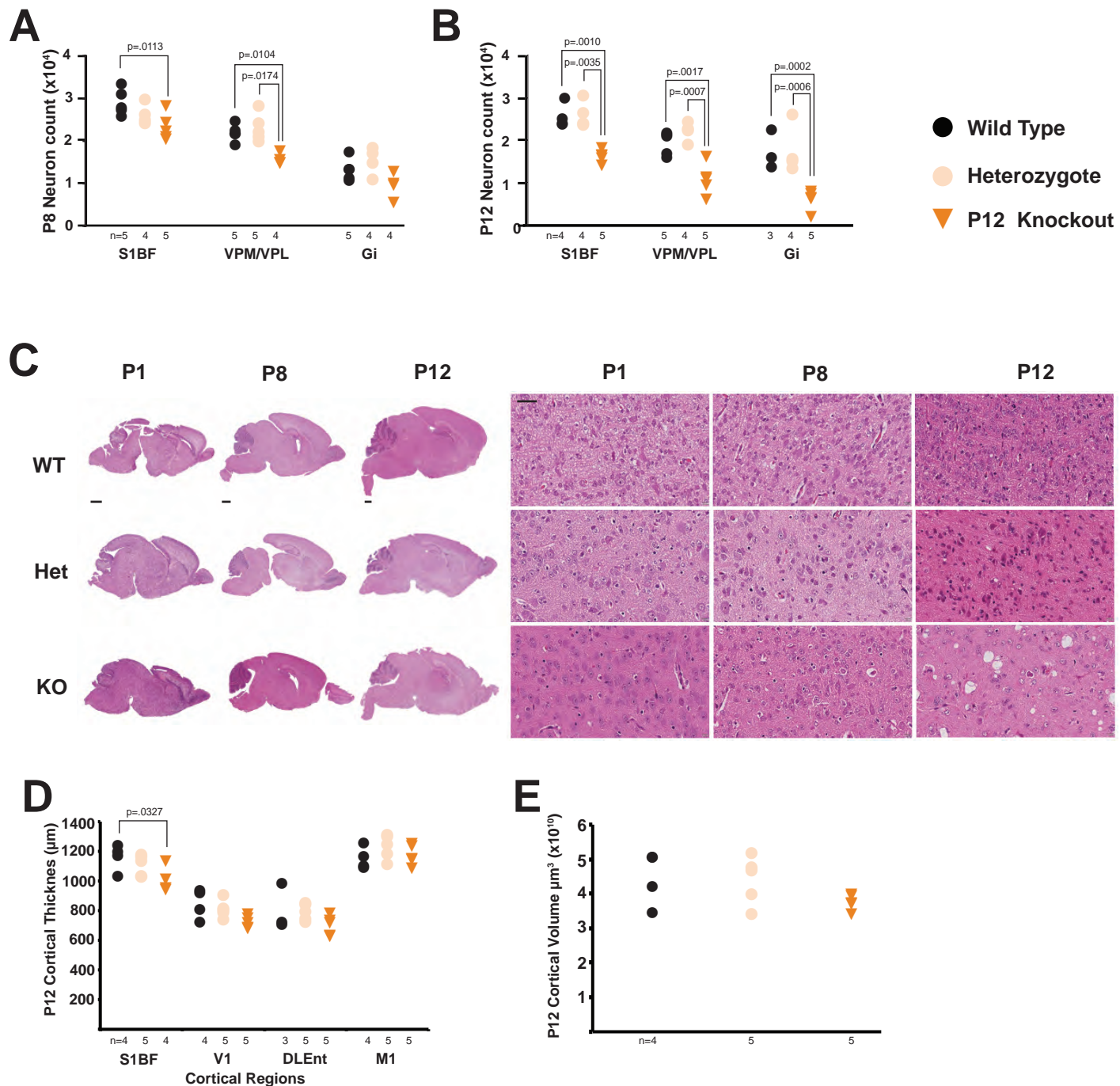
CD68 immunohistochemistry and quantification on brain sections from wildtype, heterozygous and knockout mice at P1 (A), P8 (B) and P12 (C). Whole brain scale bar = 1mm; high magnification sections scale bar = 0.25mm, (2-way ANOVA, Tukey's multiple comparison). Scale bars = 0.25mm. (D) Iba1 immunohistochemistry at P1, at P8 (E), and P12 (F) in sagittal paraffin embedded sections. Whole brain scale bar = 0.5mm; high magnification sections scale bar = 40 μ m. Numbers of mice are stated under each group. n.s. = not significant

Supplementary Fig. 2



Supplementary Fig. 2. Astrogliosis in nGD mice.
 GFAP immunohistochemistry and quantification on brain sections from wildtype, heterozygous and knockout mice at P1 (A), P8 (B) and P12 (C). Whole brain scale bar = 1mm; high magnification sections scale bar = 0.25mm (2-way ANOVA, Tukey's multiple comparison, n=4-5 mice). Scale bars = 0.25mm. Numbers of mice are stated under each group. n.s. = not significant

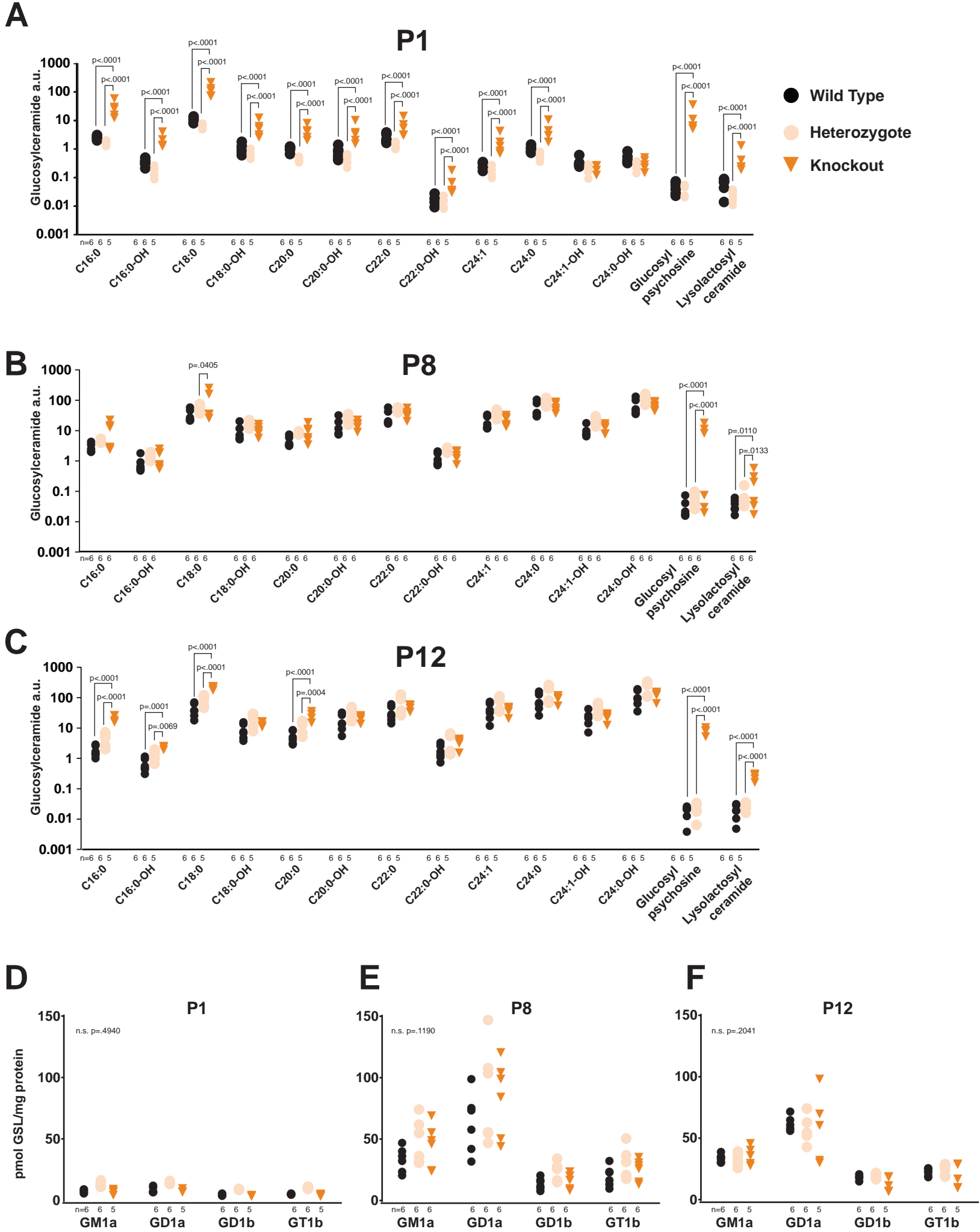
Supplementary Fig. 3



Supplementary Fig. 3. Histological and stereological analysis of nGD mouse brains.

Stereological counts of neurons in brain sections from (A) P8 and (B) P12 knockouts, heterozygous and wildtypes (2-way ANOVA, Tukey's multiple comparison). (C) Haematoxylin and eosin staining of P1, P8 and P12 brains. Whole brain scale bar = 0.5mm; high magnification sections scale bar = 40 μm . (D) Cortical thickness and (E) cortical volume measurements from P12 mice (Students one-tailed t-test). Numbers of mice are stated under each group. n.s. = not significant

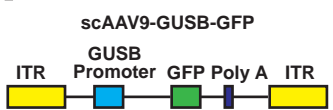
Supplementary Fig. 4



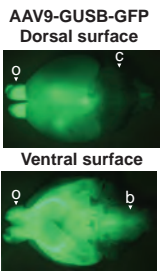
Supplementary Fig. 4. Metabolite and glycosphingolipid profile analysis of nGD mouse brains.
 (A) Mass spectrometry of P1, (B) P8 and (C) P12 brains from knockout, heterozygous and wildtype mice (2-way ANOVA on log-transformed data, n=5 vs. 6 mice; Bonferroni's multiple comparison). The glycosphingolipid profiles of GM1a, GD1a, GD1b and GT1b were measured in (D) P1, (E) P8 and (F) P12 brains (2-way ANOVA on log-transformed data, n=5 vs. 6 mice; Bonferroni's multiple comparison). Numbers of mice are stated under each group. n.s. = not significant

Supplementary Fig. 5

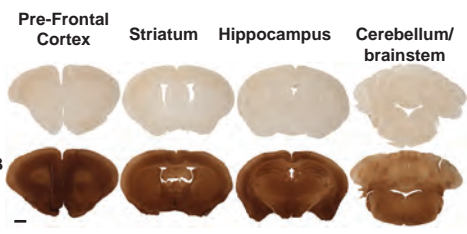
A



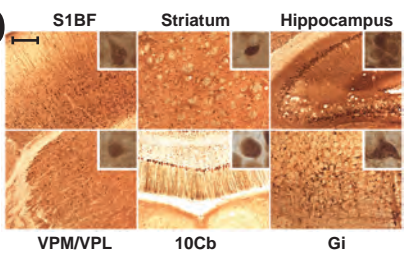
B



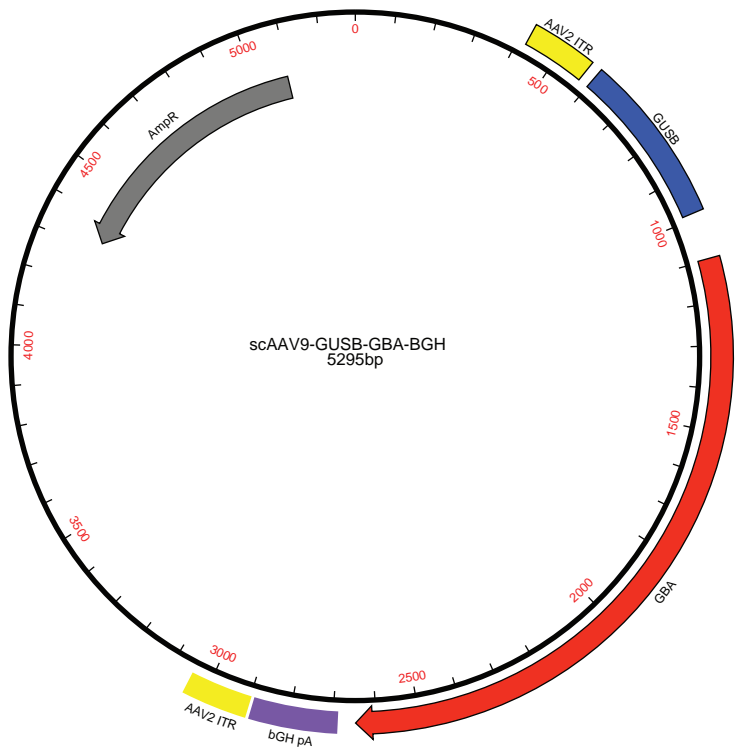
C



D



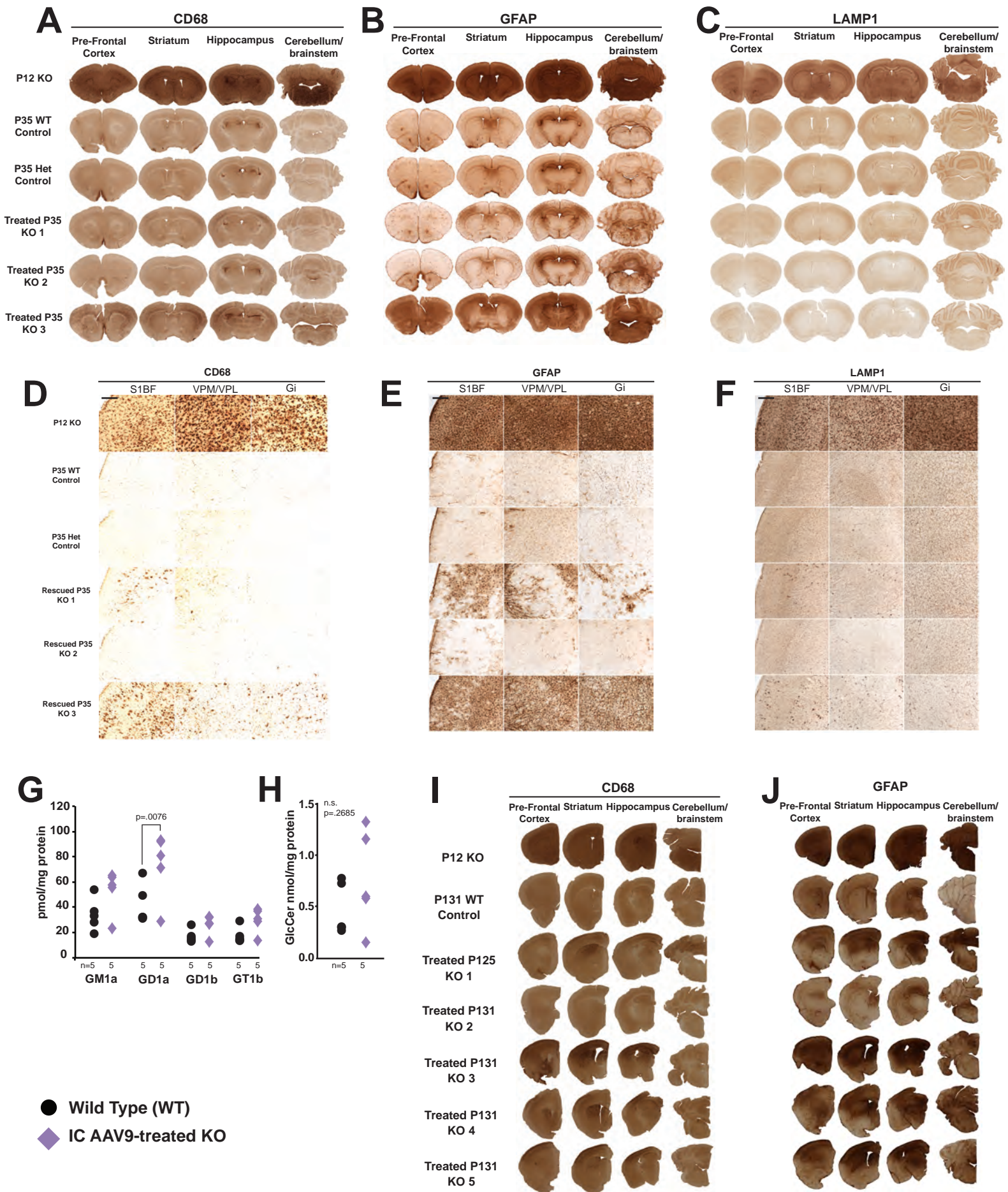
E



Supplementary Fig. 5. Fetal gene delivery marker gene studies in wild type mice.

(A) An illustration of the self-complementary genome configuration of AAV9-GUSB-GFP. The expression cassette contained the beta-glucuronidase promoter driving expression of the GFP gene followed by a polyadenylation signal. The expression cassette was flanked by the viral inverted terminal repeats. (B) Green fluorescent protein in administered brains (o-olfactory bulbs, b-brainstem, c – cerebellum). Low (C) and high (D) magnification images following anti-GFP immunohistochemistry of free-floating brain sections. Whole brain scale bar = 1mm; high magnification sections scale bar = 0.25mm. Representative of 3 administered and unadministered mice replicates. (E) Plasmid map of AAV9-GUSB-GBA.

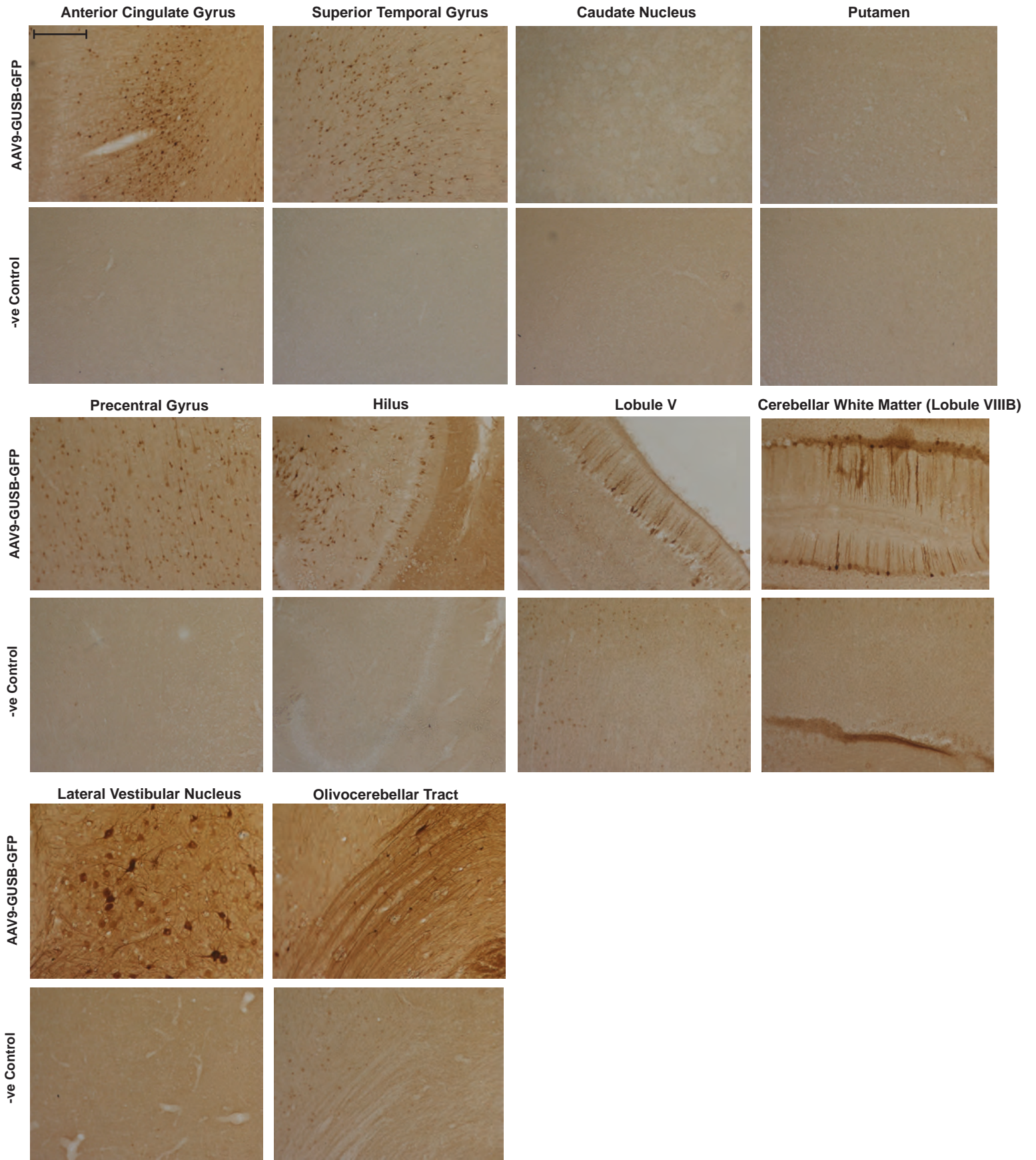
Supplementary Fig. 6



Supplementary Fig. 6. Fetal gene therapy of nGD mice neuropathology.

(A and D) CD68, (B and E) GFAP and (C and F) LAMP1 immunostaining on brain sections of P12 untreated knockouts, P35 wildtypes and heterozygous and gene therapy treated knockouts. Scale bars = 0.25mm. Representative of 3 mice replicates per experimental cohort. (G) Analysis of GLS in treated mice and control wild types, (2-way ANOVA on log-transformed data; Bonferroni's multiple comparison). (H) Glucosylceramide levels in the brains of treated knockouts and wildtypes from long term studies (Students one-tailed t-test, n=5 mice). (I) CD68 and (J) GFAP immunostaining on brain sections from long term treated knockouts and wild type mice (all replicates shown). Numbers of mice are stated under each group. n.s. = not significant

Supplementary Fig. 7



Supplementary Fig. 7. Fetal gene delivery marker gene studies in macaques.

GFP immunohistochemistry to detect cells transduced with scAAV9-GUSB-GFP following ultrasound-guided intracerebroventricular injection of to the fetal macaque. Scale bar = 0.25mm. Representative of two replicates.

Supplementary Fig. 8

TCGCGCGTTTTCGGTGATGACGGTGAAAACCTCTGACACATGCAGCTCCCGGAGACGGTCACAGCTTGTCTGTAAGCGGATGCCGGGAGCAGACAAGCCCCGTAGGGCGC
GTCAGCGGGTGTGGCGGGTGTGGGGCTGGCTTAACTATGCGGCATCAGAGCAGATTGACTGAGAGTGCACCATATGCGGTGTGAAATACCGCACAGATGCGTAAGGA
GAAAATACCGCATCAGGCGCCATTGCGCATTAGGCTGCGCAACTGTTGGGAAGGGCGATCGGTGCGGGCCTCTTCGCTATTACGCCAGCTGGCGAAAAGGGGGATGTGC
TGCAAGGCGATTAAGTTGGGTAACGCCAGGGTTTTCCAGTCACGACGTTGTA AACGACGGCCAGTGAATTCGAGCTCGGTACCTCGCGAATGCATCTAGAGGCCACTC
CCTCTGCGCGCTCGCTCGTCACTGAGGCCGGGCGACCAAAGGTCGCCCCGACGCCCGGGCTTTCGCCGGGCGCCTCAGTGAAGCGAGCGAGCGCGCAGAGAGGGA
GTGGCCAACTCCATCACTAGGGGTTCTGGAGGGGTGGAGTCGTGACAGATCTGAATTCCTGCTGGGAAAAGCAAGTGGAGGTGCTCCTGAAGAAAACAGGGGGATCC
ACCGATCTCAGGGGTTCTGTTCTGGCCTGCGGCCCTGGATCGTCCAGCCTGGGTGCGGGTGGGGAGCAGACCTCGCCCTTATCGGCTGGGGTGGGGTGGGGTCCCC
TTTCCCAAAGGCCTAGCCTGGGGTCCAGCCACAAGCCCTACCGGGCAGCGCCCGGCCCTCCAGGCCTGGCACTCGTCTCAACCAAGATGGCGCGGATGGC
TTCAGGCGCATCACGACACCGGCGCGTCACGCGACCCGCCCTACGGGCACCTCCCGCGTTTTCTTAGCGCCGACAGCGGTGGCCGAGCGGGGACC GGGAAGCATGG
CCCCGGCTGCAGCTCTAAGGTAAATATAAAATTTTTAAGTGTATAATGTGTTAAACTACTGATTCTAATTGTTCTCTCTTTTAGATTCCAACCTTTGGA ACTCAATTCAGCCA
CCATGGCTGGCAGTCTTACAGGTCTCTGCTCCTGCAAGCTGTCTCTGGGCTTCTGGGGCCAGGCCCTGTATCCCAAATCCTTTGGATACTCATCTGTGGTGTGTGTTG
TAATGCCACTTATTGTGATAGCTTTGACCCCCCACCCTTCTGCACTGGGCACCTTTTCAAGGTATGAATCTACCAGGTCTGGGAGGAGGATGGAGCTGAGTATGGGGCC
CATCAAGCAAACCTACTGGCACTGGCTTGTGCTGACACTGCAACTGAACAGAAAGTTCAGAAAAGTGAAGGGCTTTGGAGGAGCCATGACTGATGCTGCTGCCCTC
AATATTTTGGCCCTGAGCCCCCTGCTCAGAATCTCCTTTTGAATCATACTTCTGAGGAGGGAATTGGATACAATATCATCAGGGTGCCAATGGCCTCATGTGACTTTAG
TATTAGGACTTACACCTATGCTGATAACCCTGATGATTTCCAGCTGCATAACTTCTCATTGCCTGAGGAGGATACCAAATGAAGATCCCCTACTTACAGGGCCCTGCAAC
TGGCTCAGAGACCAGTGTCAATTGCTGGCCTCCCCCTGGACCTCCCCA ACTGGCTCAAACCAATGGGGCTGTCAATGGTAAGGGCTCTTTAAGGGGCGAGCCTGGAGAC
ATTTACCATCAGACCTGGGCCAGGATTTTTGTGAAGTTCCTGGATGCTTATGCTGAGCACA AATTGCAATTTTGGGCTGTTACAGCTGAGAATGAACCTCTGCAGGACTG
CTGTCTGGCTATCCTTTCCAGTGCCTGGGCTTTACCCCTGAGCATCAGAGGGATTTTATTGCCAGGGACCTGGGACCTACTCTTGCCAATAGCACACACCATAATGTGAGG
CTTCTGATGCTTATGACAGAGACTTCTGCTGCCACACTGGGCCAAGGTTGTCCTGACAGATCTGAGGCTGCCAAGTATGTTTATGGGATTGCTGTGCACTGGTATCTG
GACTTCTTGTCCAGCTAAGGCCACCCTGGGAGAAAACACAGGTTGTTTTCCAAATACAATGCTTTTTGCATCAGAGGCCTGTGTGGGCAGTAAATTTTGGGAGCAGTC
TGTTAGGCTGGGGAGCTGGGATAGAGGAATGCAATACTCCATTCTATCATACCAATCTGCTTACCATGTGGTGGGGTGGACTGACTGGAACCTTGCCCTTAAACCTGA
GGGTGGCCCCAATTGGGTCAGGAATTTTGTGGATAGTCCCATTGTGGATACCAAGGACACATTCTATAAGCAACCAATGTTCTATCACCTGGGTCACTTTAGTAAGT
TTATCCCTGAGGGGTCCCAGAGGGTGGGACTGGTGGCTTCCAGAAGAATGATCTGGATGCTGTGGCCCTGATGCACCCTGATGGCAGTGTGTGGTTGTTGTTCTCAATA
GAAGCTCTAAAGATGTGCCCTTGACCATCAAAGATCCAGCTGTGGGATTTCTGGAACA AATTTCCCTGTTTATAGCATCCACACTTACCTTTGGAGAAGGCAGTGAAAA
GAAGGCCTGATAATTGCACCACCAGGCCTGATAGGCCCTGTGCCCTTAGTGGCAGCCATCTGTTGTTTGGCCCTCCCCGTGCCTTCTTGACCCTGGAAGGTGCCACTC
CCACTGTCTTTCTAATAAAATGAGGAAATTGCATCGCATTGTCTGAGTAGGTGTCACTTATTCTGGGGGTGGGGTGGGGCAGGACAGCAAGGGGGAGGATTGGGAA
GACAATAGCAGGCATGCACTAGTCCACTCCCTCTGCGCGCTCGCTCGCTCACTGAGGCCGGGCGACCAAAGGTCGCCCGACGCCCGGGCTTTGCCCGGGCGGCCTCA
GTGAGCGAGCGAGCGCGCAGAGAGGGATCTAGATATCGGATCCCGGGCCCGTGCAGTGCAGAGGCCTGCATGCAAGCTTGGCGTAATCATGGTCATAGCTGTTTCTGTG
TGAAATGTTATCCGCTCACAATCCACACAACATACGAGCCGGAAGCATAAAAGTGTAAAGCCTGGGGTGCCTAATGAGTGAGCTAACTCACATTAATTGCGTTGCGCTCAC
TGCCCGCTTTCCAGTCGGGAAACCTGCTGTGCCAGCTGCATTAATGAATCGGCCAACGCGCGGGGAGAGGCGGTTTGCATTGGGCGCTCTTCCGCTTCTCGCTCACT
GACTCGCTGCGCTCGGTGCTTGGGCTGCGGCGAGCGGTATCAGCTCACTCAAAGGCGGTAATACGGTTATCCACAGAATCAGGGGATAACGCAGGAAAAGAACATGTGAG
CAAAGGCCAGCAAAGGCCAGGAACCGTAAAAAGGCCGCTTGTGGCGTTTTTCCATAGGCTCCGCCCCCTGACGAGCATCACAAAATCGACGCTCAAGTCAGAG
GTGGCGAAACCCGACAGGACTATAAAGATAACAGGCGTTTTCCCTGGAAGCTCCCTCGTGCCTCTCTGTTCCGACCTGCGCTTACCGGATACCTGTCCGCCTTTCTC
CCTTCGGGAAGCGTGGCGCTTTCTCATAGCTCACGCTGTAGGTATCTAGTTCGGTGTAGGTGCTTGCCTCAAGCTGGGCTGTGTGCACGAACCCCCCGTTACGCCGAC
CGCTGCGCCTTATCCGGTAACTATCGTCTTGAAGTCCAAACCGGTAAGACACGACTTATCGCCACTGGCAGCAGCCACTGGTAACAGGATTAGCAGAGCGAGGTATGTAGG
GGTGTACAGAGTTCTGAAGTGGTGGCCTAACTACGGCTACACTAGAAGAACAGTATTTGGTATCTGCGCTCTGCTGAAGCCAGTTACCTTCGGAAAAAGAGTTGGTAG
CTCTTGATCCGGCAAACAACCACCGCTGGTAGCGGTGGTTTTTTTTGTTTGAAGCAGCAGATTACGCGCAGAAAAAAAGGATCTCAAGAAGATCCTTTGATCTTTTCTAC
GGGGTCTGACGCTCAGTGGAAACGAAAACCTACGTTAAGGGATTTTGGTATGAGATTATCAAAAAGGATCTTACCTAGATCCTTTTAAATAAAAATGAAGTTTTAAATCA
ATCTAAAGTATATAGTAAACTTGGTCTGACAGTTACCAATGCTTAATCAGTGAGGCACCTATCTCAGCGATCTGTCTATTTCTGTTTACCTATAGTTGCTGACTCCCCGCT
GTGTAGATAACTACGATACGGGAGGGCTTACCATCTGGCCCCAGTGTGCAATGATACCGCGAGACCCACGCTACCCGGCTCCAGATTTATCAGCAATAAACCAGCCAGCC
GGAAGGGCCGAGCGCAGAAGTGGTCTGCAACTTTATCCGCTCCATCCAGTCTATTAATTGTTGCCGGGAAGCTAGAGTAAGTAGTTCGCCAGTTAATAGTTTGGCGAAC
GTTGTTGCCATTGCTACAGGCATCGTGGTGTACGCTCGCTGTTGGTATGGCTTCATCAGCTCCGGTCCCAACGATCAAGGCGAGTTACATGATCCCCCATGTTGTGCA
AAAAAGCGGTTAGCTCCTTCGGTCTCCGATCGTTGTGAGAAAGTAAAGTGGCCGAGTGTATCACTCATGGTTATGGCAGCACTGCATAATTCTCTTACTGTATGCCATCC
GTAAGATGCTTTTCTGTGACTGGTGAAGTACTCAACCAAGTCATTCTGAGAATAGTGTATGCGGCGACCGAGTTGCTCTTGGCCGGGCTCAATACGGGATAATAACCGCGCCAC
ATAGCAGAACTTTAAAAGTGTCTATCATTGAAAACGTTCTCGGGGCGAAAACCTCAAGGATCTTACCGCTGTTGAGATCCAGTTTCATGTAACCCACTCGTGCACCCA
ACTGATCTTACGATCTTTTACTTTCACCAGCGTTTCTGGGTGAGCAAAAACAGGAAGGCAAAATGCCGCAAAAAAAGGGAATAAGGGCGACACGGAAATGTTGAATACT
CATACTCTTCTTTTCAATATTATTGAAGCATTATCAGGGTTATTGTCTCATGAGCGGATACATATTTGAATGATTTAGAAAAATAAACAAATAGGGGTTCCGCGCACATTT
CCCCGAAAAGTGCCACCTGACGTCTAAGAAACCATTATTATCATGACATTAACCTATAAAAATAGGCGTATCACGAGGCCCTTTCGTC

Supplementary Fig. 8. Sequence of scAAV9-GUSB-GBA

Supplementary Table 1

CD68

	1	8	12		1	8	12
Cortex				Midbrain			
Frontal Association	-/+	++	+++	Red Nucleus	-	++	+++
Motor	+	++	+++	Superficial Area of Superior Colliculus (SC)	-	+	+
Sensory	-/+	++	++++	Intermediate and Deep Layers of SC	-	+//++	++
Piriform	-/+	++	+++	Periaqueductal Gray	-	+//++	++
Auditory	-/+	++	+++	Inferior Colliculus	-	++	+++
Visual	-/+	++	+++				
CEnt	-/+	++	+++				
Basal Ganglia				Pons & Medulla			
Caudate Putamen	-	++	++	Reticulotegmental Nucleus of Pons	+//++	+++	++++
Globus Pallidus	-	++	+++	Pontine Reticular Nucleus	+//++	+++	++++
Substantia Nigra	-	++	+++	Ventral Cochlear Nucleus	+/-	++	+++
Hippocampus				8 Nerve	-	-	+
CA1	-	+	+++	Facial Nucleus	-	-	+
CA2/CA3	-	+	+++	Vestibular Nucleus	-	+	++
Dentate Gyrus	-	-	-	External Cuneate	-	++	+++
Dorsal Subiculum	-	+	+++	LRT	+	+++	++++
Hypothalamus				Parvicellular Reticular Nucleus (PCRt)	+	+++	++++
Anterior Hypothalamic Area	+	++	+++	Motor Trigeminal Nucleus	-	++	+++
Lateral Nucleus	+	++	+++//++++	Motor Root of the Trigeminal Nerve	+	+++	++++
Medial Pre-Optic Nucleus	+	+++//+++	+++	Peripheral Sensory Trigeminal Nucleus	-	++	+++
Ventromedial Nucleus	+/-	++	+++	SP5	-	++	+++
Mammillary Nucleus	+/-	++	+++	Dorsal Motor Nucleus Of Vagus	-	+	+++
Thalamic Nuclei				Hypoglossal Nucleus	+	++	++++
Anteroventral	+	++	++++	Gigantocellular Nucleus	++	+++	++++
Anterodorsal	+	++	++++				
Paraventricular	-	++	+++//+++				
Reticular	-	++	+++				
Ventral Post Medial/	+	+++	++++				
Ventral Post Lateral							
Mediodorsal	+/-	++	+++//++++				
Habenular	-	+	++				
Laterodorsal	+/-	++	+++				
Posterior							

Supplementary Table 1. Scoring of CD68 immunohistochemistry in the nGD mouse model.

Discrete areas of the brain in knockout, wild type and heterozygous mice were scored at P1, P8 and P12. A scale of - to ++++ was used, where - = no activated microglia visible and ++++ was area densely populated with activated microglia.

Supplementary Table 2

GFAP

	1	8	12		1	8	12
Cortex				Midbrain			
Frontal Association	-	++	++	Red Nucleus	-/+	++	+++
Orbital	-	++	++	Superficial Area of Superior Colliculus (SC)	-/+	++	+++
Motor	-/+	+++	+++	Intermediate and Deep Layers of SC	-/+	++	+++
Sensory	-/+	+++	+++	Periaqueductal Gray	-	++	+++
Piriform	-/+	++	+++/++++	Inferior Colliculus	-	++	+++
Auditory	-/+	++	+++				
Visual	-/+	++	+++	Pons & Medulla			
CEnt	-/+	++	+++	Reticulotegmental Nucleus of Pons	++	++	++++
Basal Ganglia				Pontine Reticular Nucleus	+	++/+++	++++
Caudate Putamen	-	+ / ++	++	Ventral Cochlear Nucleus	+	++	+++
Globus Pallidus	-	+ / ++	++/+++	8 Nerve	+	+++	++++
Substantia Nigra	-/+	++	+++	Facial Nucleus	+	+++	++++
Hippocampus				Vestibular Nucleus	-	+++	++++
CA1	+	++/+++	+++	External Cuneate	-	+++	++++
CA2/CA3	+	++/+++	+++	LRT	+	+++	++++
Dentate Gyrus	-	++/+++	+++	Parvicellular Reticular Nucleus (PCRT)	+	+++	++++
Dorsal Subiculum	-	++/+++	+++	Motor Trigeminal Nucleus	+	+++	++++
Hypothalamus				Motor Root of the Trigeminal Nerve	-/+	+++	++++
Anterior Hypothalamic Area	+	++/+++	+++	Peripheral Sensory Trigeminal Nucleus	-/+	+++	++++
Medial Pre-Optic Nucleus	-/+	++	+++	SP5	+	+++	++++
Ventromedial Nucleus	+	++	+++	Dorsal Motor Nucleus Of Vagus	++	+++	++++
Mammillary Nucleus	-	++	+++	Hypoglossal Nucleus	++/+++	+++	++++
Thalamic Nuclei				Gigantocellular Nucleus	++/+++	+++	++++
Anteroventral	++	+++	+++ / ++++				
Anterodorsal	++	+++	+++ / ++++				
Paraventricular	++	+++	+++ / ++++ +				
Ventral Post Medial/	+	+++ / ++++	++++				
Ventral Post Lateral							
Mediodorsal	+	++	+++				
Habenular	+	++	++ / +++				
Laterodorsal	+	++	+++				
Posterior	-/+	++	+++				

Supplementary Table 2. Scoring of GFAP immunohistochemistry in the nGD mouse model.

Discrete areas of the brain in knockout, wild type and heterozygous mice were scored at P1, P8 and P12. A scale of - to ++++ was used, where - = no activated astrocytes visible and ++++ was area densely populated with activated astrocytes.

Supplementary Table 3

Fold change in glycosphingolipids, KO/WT

	P1	P8	P12
C16:0	21	4	13
C16:0-OH	12	2	4
C18:0	22	4	6
C18:0-OH	10	1	2
C20:0	8	2	5
C20:0-OH	10	1	1
C22:0	5	1	2
C22:0-OH	7	1	2
C24:1	13	1	1
C24:0	8	1	1
C24:1-OH	1	1	1
C24:0-OH	1	1	1
Glucosylpsychosine	524	216	485
Lysolactosyl ceramide	15	6	14

Supplementary Table 4

Glycosphingolipid MRM transitions

Glycosphingolipid name	Precursor m/z	Fragment m/z	Cone (V)	Collision (V)
glucosylpsychosine	462.4	264.3	74	16
lyso-lactosyl ceramide	624.6	264.4	18	20
C16:0 glucosylceramide	722.6	560.6	130	40
d4C16:0 glucosylceramide	726.6	564.7	130	38
C16:0-OH glucosylceramide	738.6	264.3	130	32
C18:0 glucosylceramide	750.6	588.6	130	38
C18:0-OH glucosylceramide	766.6	264.3	130	32
C20:0 glucosylceramide	778.6	616.7	132	42
C20:0-OH glucosylceramide	794.6	264.3	132	36
C22:0 glucosylceramide	806.7	644.7	130	38
C22:0-OH glucosylceramide	820.7	658.8	130	52
C24:1 glucosylceramide	832.7	670.7	130	52
C24:0 glucosylceramide	834.7	672.7	130	42
C24:1-OH glucosylceramide	848.7	686.7	130	42
C24:0-OH glucosylceramide	850.8	688.9	130	42